Systems/Circuits

Optogenetic Stimulation of Type I GAD65$^+$ Cells in Taste Buds Activates Gustatory Neurons and Drives Appetitive Licking Behavior in Sodium-Depleted Mice

Caitlin Baumer-Harrison,[1]* Martin A. Raymond,[1]* Thomas A. Myers,[1] Kolbe M. Sussman,[1] Spencer T. Rynberg,[2] Amanda P. Ugartechea,[1] Dean Lauterbach,[1] Thomas G. Mast,[2,3] and Joseph M. Breza[1,3]

[1]Department of Psychology, College of Arts and Sciences, Eastern Michigan University, Ypsilanti, Michigan 48197, [2]Department of Biology, College of Arts and Sciences, Eastern Michigan University, Ypsilanti, Michigan 48197, and [3]Program in Neuroscience, College of Arts and Sciences, Eastern Michigan University, Ypsilanti, Michigan 48197

Mammalian taste buds are comprised of specialized neuroepithelial cells that act as sensors for molecules that provide nutrition (e.g., carbohydrates, amino acids, and salts) and those that are potentially harmful (e.g., certain plant compounds and strong acids). Type II and III taste bud cells (TBCs) detect molecules described by humans as "sweet," "bitter," "umami," and "sour." TBCs that detect metallic ions, described by humans as "salty," are undefined. Historically, type I glial-like TBCs have been thought to play a supportive role in the taste bud, but little research has been done to explore their role in taste transduction. Some evidence implies that type I cells may detect sodium (Na^+) via an amiloride-sensitive mechanism, suggesting they play a role in Na^+ taste transduction. We used an optogenetic approach to study type I TBCs by driving the expression of the light-sensitive channelrhodopsin-2 (ChR2) in type I GAD65$^+$ TBCs of male and female mice. Optogenetic stimulation of GAD65$^+$ TBCs increased chorda tympani nerve activity and activated gustatory neurons in the rostral nucleus tractus solitarius. "N neurons," whose NaCl responses were blocked by the amiloride analog benzamil, responded robustly to light stimulation of GAD65$^+$ TBCs on the anterior tongue. Two-bottle preference tests were conducted under Na^+-replete and Na^+-deplete conditions to assess the behavioral impact of optogenetic stimulation of GAD65$^+$ TBCs. Under Na^+-deplete conditions GAD65-ChR2-EYFP mice displayed a robust preference for H_2O illuminated with 470 nm light versus nonilluminated H_2O, suggesting that type I glial-like TBCs are sufficient for driving a behavior that resembles Na^+ appetite.

Key words: **GAD65; nucleus tractus solitarius; optogenetics; preference; sensory systems; taste**

Significance Statement

This is the first investigation on the role of type I GAD65$^+$ taste bud cells (TBCs) in taste-mediated physiology and behavior via optogenetics. It details the first definitive evidence that selective optogenetic stimulation of glial-like GAD65$^+$ TBCs evokes neural activity and modulates behavior. Optogenetic stimulation of GAD65$^+$ TBCs on the anterior tongue had the strongest effect on gustatory neurons that responded best to NaCl stimulation through a benzamil-sensitive mechanism. Na^+-depleted mice showed robust preferences to "light taste" (H_2O illuminated with 470 nm light vs nonilluminated H_2O), suggesting that the activation of GAD65$^+$ cells may generate a salt-taste sensation in the brain. Together, our results shed new light on the role of GAD65$^+$ TBCs in gustatory transduction and taste-mediated behavior.

Received Mar. 12, 2020; revised Aug. 17, 2020; accepted Aug. 23, 2020.

Author contributions: C.B.-H., M.A.R., T.G.M., and J.M.B. designed research; C.B.-H., M.A.R., T.A.M., K.M.S., S.T.R., A.P.U., T.G.M., and J.M.B. performed research; C.B.-H., M.A.R., T.A.M., K.M.S., D.L., and C.B.-H., M.A.R., T.G.M., and J.M.B. wrote the paper.

This work was supported by National Institutes of Health Grant R21 DC016990 to J.M.B., and start-up funds from Eastern Michigan University to T.G.M. and J.M.B. We thank Dr. Christopher Schatschneider (Florida State University, Tallahassee, FL) for expert advice on statistical comparisons. We also thank Dr. Kenneth Rusiniak (Eastern Michigan University) for expert advice on behavioral experiments.

*C.B.-H. and M.A.R. contributed equally to this work.

The authors declare no competing financial interests.

Correspondence should be addressed to Joseph M. Breza at jbreza1@emich.edu.

https://doi.org/10.1523/JNEUROSCI.0597-20.2020

Introduction

Mammalian taste systems detect chemicals that lead to the perception of at least five basic taste qualities. Taste transduction begins within taste bud cells (TBCs) that express receptors for carbohydrate, metallic ion, acid, alkaloid, and amino acid detection. TBCs transmit this information to neurons in cranial nerves (VII, IX, or X), which then project to the nucleus tractus solitarius (NTS) in the brainstem (Contreras et al., 1982). The molecular identity and physiology of most TBCs are well understood, with the notable exception of those responsible for salt-taste transduction.

This is an unfortunate gap, as taste provides unique information for organismal health and survival.

Three types of TBCs have been identified (types I, II, and III), and, of the three, only type I glial-like cells have yet to be unequivocally paired with a clear role in taste physiology and behavior. Type II cells express receptors for detecting molecules described by humans as "sweet," "bitter," or "umami." Type III cells are responsible for detecting acids described as "sour" (Huang et al., 2006; Teng et al., 2019) and ions described as "salty" through an amiloride-insensitive mechanism (Oka et al., 2013; Lewandowski et al., 2016; Roebber et al., 2019). Na^+ detection, discrimination, and appetite are dependent on amiloride-sensitive channels (Hill et al., 1990; Spector et al., 1996; Roitman and Bernstein, 1999; Geran and Spector, 2000, 2004). Vandenbeuch et al. (2008) recorded from isolated fungiform TBCs and suggested that those with amiloride-sensitive currents were type I cells. Extracellular recordings from intact fungiform papillae showed that TBCs narrowly tuned to NaCl (unresponsive to KCl) were amiloride sensitive (Yoshida et al., 2009). Single-unit recordings from chorda tympani neurons (which innervate fungiform papillae) showed that neurons narrowly tuned to Na^+ salts were attenuated by amiloride (Lundy and Contreras, 1999) or benzamil, an amiloride analog (Breza et al., 2010; Breza and Contreras, 2012a,b).

The taste system is essential for detecting and discriminating sodium (Na^+) from other cations. Detection thresholds and logistic functions for Na^+ and ammonium (NH_4^+) are highly similar (Geran and Spector, 2007), but neurons responding best to Na^+ are amiloride/benzamil sensitive, whereas neurons responding best to NH_4^+ are amiloride/benzamil insensitive (Lundy and Contreras, 1999; Breza and Contreras, 2012a). NH_4^+ is a toxic metabolic waste product and consumption is generally avoided, whereas Na^+ is an essential nutrient and drives taste-guided behaviors. Na^+ overconsumption in industrialized nations has led to health consequences (Gleiberman, 1973). Thus, understanding Na^+ taste physiology could ameliorate Na^+-induced disease without reducing food palatability.

We reasoned that the missing function for type I glial-like TBCs and our incomplete understanding of TBCs responsible for amiloride/benzamil-sensitive salt-taste transduction was not coincidental. We hypothesized that type I TBCs in fungiform papillae were sufficient for activating gustatory neurons that responded best to NaCl through a benzamil-sensitive mechanism. To test whether stimulation of type I TBCs served a sufficient role in salt-taste physiology and behavior, we took an optogenetic approach and drove the expression of channelrhodopsin-2 (ChR2) and enhanced yellow fluorescent protein (EYFP) in type I TBCs via the GAD65 promoter, an enzyme exclusively expressed by type I TBCs (Dvoryanchikov et al., 2011).

First, we combined optogenetic stimulation of GAD65$^+$ TBCs with electrophysiological recordings of the chorda tympani nerve (CT) and from single neurons in the rostral NTS (rNTS). Next, we reasoned that if GAD65$^+$ TBCs were capable of driving Na^+ taste, then they would be sufficient for Na^+-dependent ingestive behaviors (Roitman and Bernstein, 1999). We then used light to stimulate GAD65$^+$ TBCs in a drinking assay in Na^+-depleted mice. The optogenetic approach allowed for us to selectively stimulate GAD65$^+$ TBCs without the confounding influences of somatosensation, olfaction, or osmotic pressure—variables typically inherent to taste solutions. Additionally, mice expressing ChR2 in GAD65$^+$ TBCs displayed a robust preference for illuminated H_2O versus nonilluminated H_2O while in a Na^+-depleted state—a behavior that largely recapitulated Na^+ appetite. Together, our results shed light on the function of type I glial-like TBCs in taste-mediated physiology and behavior.

Materials and Methods

Animals

All experiments were conducted in compliance with the Eastern Michigan University Institutional Animal Care and Use Committee. A total of 107 mice (54 male and 53 female) were used in these studies. Mice were housed in polycarbonate cages bedded with corncob, with free access to food (Labdiet 5015; 0.43% Na^+) and tap H_2O, and kept on a reverse 12 h light/dark cycle in a temperature- and humidity-controlled room. Homozygous GAD65cre (catalog #010802) and Ai32 homozygous for the Rosa-CAG-LSL-ChR2(H134R)-EYFP-WPRE conditional allele (catalog #012569) mice were purchased from The Jackson Laboratory and served as homozygous breeders. The offspring of these mouse lines were cross bred (GAD65cre × Ai32) to produce heterozygous mice to liberate the expression of ChR2 and EYFP in GAD65$^+$ cells (GAD65-ChR2-EYFP). C57BL/6J mice [wild type (WT)] were also purchased from The Jackson Laboratory and bred in the vivarium at Eastern Michigan University.

Tissue preparation

Mice were administered isoflurane gas for initial sedation and deeply anesthetized with an intraperitoneal injection of urethane (1.5 g/kg). Mice were then perfused intracardially with 1× PBS, pH 7.4, followed by ice-cold PFA (Acros Organics) dissolved in PBS (4% PFA/PBS, pH 7.4). Tongues were extracted and postfixed in 4% PFA/PBS for 2 h and transferred to 30% sucrose/PBS solution for storage at 4°C until sectioning. Tongues were dissected from the mandible, caudal to the circumvallate papillae, and the anterior portion was prepared for sectioning in optimal cutting temperature (OCT) compound (Sakura Finetek). Using an International Equipment Company Minotome Cryostat at −18°C, tongues were sectioned at 8 µm and placed onto gelatin-coated slides. Slides were stored at −20°C until immunohistochemistry was performed.

Immunohistochemistry

To validate the expression pattern of EYFP in taste buds, the following three different primary antibodies were used: rabbit anti-mouse NTPDase2 (from Julie Pelletier, University of Laval, Quebec City, QC, Canada); rabbit anti-PLCβ2 (Q-15; catalog #SC-206, Santa Cruz Biotechnology); and goat anti-carbonic anhydrase IV/CA4 antigen affinity-purified polyclonal antibody (CA4; catalog #AF2414, R&D Systems). NTPDase2 is a marker for type I cells (Bartel et al., 2006; Dvoryanchikov et al., 2011), PLCβ2 for type II cells, and CA4 for type III cells. Frozen sections on slides were air dried briefly and rehydrated with PBS in a series of four rinses for a total of 1 h. Sections were permeabilized in 1% PBST (Triton X-100 in PBS) for 25 min, followed by 5% normal donkey serum (NDS) in 0.3% PBST blocking solution for 2 h. All antibodies were titrated in half log concentration steps. The appropriate primary antibody for NTPDase2, PLCβ2, and CA4 was diluted at the appropriate concentration (1:1000, 1: 2000, or 1: 1500, respectively) in the blocking solution and incubated for 24–72 h at 4°C.

Slides were then thoroughly rinsed with PBS in a series of nine rinses over 90 min to remove the primary antibody. The appropriate secondary antibody [Donkey Anti-Goat IgG H&L Texas Red (catalog #ab6883, Abcam); or Donkey Anti-Rabbit IgG H&L Texas Red (catalog #ab6800, Abcam)] was diluted in donkey serum and applied to the slides for 3 h. The secondary was rinsed briefly with 1× PBS and DAPI (1:20,000), a fluorescent stain that binds to DNA, was applied for 5 min. DAPI was rinsed off with 1× PBS and slides were allowed to air dry overnight. Once dry, slides were coverslipped using Vectamount (Vector Laboratories). Fluorescent photomicrographs were first taken at 40× and then at 100× (oil-immersion) using a Nikon Eclipse E400 Microscope with a CoolSNAP MYO camera. Images were viewed using NIS Elements software and stored on a computer for analysis.

Surgical procedures

Transgenic mice were administered isoflurane gas for initial sedation and deeply anesthetized with injections of urethane (1.5 g/kg, i.p.).

Supplemental doses were administered accordingly based on reflexive responses. To facilitate breathing, mice were then tracheostomized with a stainless steel cannula. Body temperature was maintained at 37°C with a custom-made (from Paul Hendrick, Florida State University, Tallahassee, FL) heating pad and temperature controller.

For CT nerve recordings, mice were placed in a custom-made brass head holder (from J.M.B.), which could be rotated for the nerve dissection. The whole CT nerve was exposed by a mandibular approach, transected proximally, and desheathed for recording as described previously (Breza and Contreras, 2012a,b; Lu et al., 2012, 2016).

For single-unit recordings, mice were placed in a custom-built stereotaxic apparatus (from J.M.B.) and their heads secured with adjustable ear cuffs. A midline incision was made in the skin overlying the cranium, and connective tissue was removed from the surface of the skull. A portion of the occipital bone was drilled away with a dental burr to allow access to the cerebellar surface.

Neurophysiology

CT nerve

The CT nerve was cut near its entrance into the tympanic bulla and draped over a platinum wire hook (positive polarity), and the entire cavity was then filled with paraffin oil (VWR) to isolate the signal from ground and maintain nerve integrity. An indifferent electrode (negative polarity) was attached to the skin overlying the cranium with a stainless steel wound clip. Neural activity was differentially amplified [bandpass 300–5000 Hz; alternating current (AC) × 10,000; A-M Systems], observed with an oscilloscope, digitized with waveform hardware and software (Spike 2, Cambridge Electronic Design), integrated using the root mean square method (500 ms time constant), and stored on a computer for offline analysis.

Single-unit recordings

Glass-insulated tungsten electrodes (Z = 1–3 MΩ) were used to record single-unit activity and were lowered into the cerebellum at 0°. An indifferent electrode was attached to the skin overlying the posterior cranium. Neural activity was differentially amplified (bandpass 300–5000 Hz; AC × 10,000; A-M Systems), observed with an oscilloscope and audiomonitor, digitized with waveform hardware and software (Spike 2; Cambridge Electronic Design), and stored on a computer for analysis. After the electrode transitioned out of vestibular nuclei (typically, ~3800–4100 μm), we tested the oral cavity and surrounding regions for mechanosensory (using a blunt-glass probe), gustatory (taste solutions; see Stimulation procedures), and light sensitivity to determine where our recording electrode was relative to the anterior tongue region of the gustatory NTS medial to the "transition zone" as described previously (Breza and Travers, 2016). If we encountered mechanosensory units, the electrode was then retracted and moved medially, and the procedure was repeated until we encountered gustatory neurons with receptive fields confined to the anterior tongue that were devoid of tactile sensitivity. We limited taste-receptive fields to the anterior tongue, because chorda tympani neurons that innervate this region are critical for normal salt detection (Spector et al., 1990), salt discrimination (Spector and Grill, 1992; Blonde et al., 2010), and Na^+ appetite (Roitman and Bernstein, 1999). Once a gustatory neuron in the NTS was isolated, we began taste and light-stimulation procedures (see Stimulation procedures). This was repeated for as many neurons as we could possibly isolate in a single animal.

Stimulation procedures

All solutions were presented to the tongue at a constant flow rate (100 μl/s) and temperature (35°C ± 0.3) by an automated commercial fluid delivery system and heated perfusion cube (OctaFlow; ALA Scientific Instruments). Artificial saliva (15 mM NaCl, 22 mM KCl, 3 mM $CaCl_2$, and 0.6 mM $MgCl_2$, dissolved in deionized H_2O) served as the rinse and solvent for all solutions (Breza et al., 2010; Breza and Contreras, 2012a,b). The tongue was adapted to 35°C artificial saliva for at least 60 s, before the start of the protocol, and between the presentation of each taste solution (0.2 M sucrose, 0.1 M NaCl, 0.01 M citric acid, 0.01 M quinine hydrochloride (QHCl), 0.1 M ammonium chloride (NH_4Cl), and NaCl + 5 μM benzamil for single units). There was an uninterrupted flow from artificial saliva to a taste stimulus, so that the temperature and flow rate remained constant. This method of delivery eliminates tactile and thermal transients during rapid switching between rinse and taste delivery. Each taste solution was presented for 10 s and signaled by square waves (see Figs. 2, 4), and were followed by a 60 s rinse.

These stimuli (basic taste stimuli and benzamil) and methods of delivery (rinse composition, temperature, and flow rate) are nearly identical to those used to categorize peripheral gustatory neurons in rats (Breza et al., 2010; Breza and Contreras, 2012a,b). Similar concentrations of basic taste stimuli have been used to categorize gustatory nerve fibers in the mouse chorda tympani (Ninomiya et al., 1982) and mouse NTS (Lemon and Margolskee, 2009; Wilson et al., 2012; Kalyanasundar et al., 2020). Here we used 0.2 M sucrose because it was less viscous than 0.3 M sucrose and evoked similar neural responses. The bitter stimulus, 0.01 M QHCl, was chosen for consistency with the Lemon and Margolskee (2009) study in the mouse NTS.

Light was delivered through the optic fiber by an LED (470 nm) and controller (catalog #OGK-0470–0200-37–250-BLSSA02, Mightex). Pulse duration and pulse frequency were controlled by a stimulator via transistor-transistor logic (TTL; catalog #S44, Grass Instruments), whereas light power (in mW) was controlled by Mightex software. Light pulses were signaled via TTL pulses to Spike2 (trigger; see Figs. 2, 6) to indicate precise onset (precision within 2 ms). During the light protocol, brief pulses (1 ms) of 470 nm light were directed at the receptive field of the anterior tongue using an optic fiber [200 μm, numerical aperture (NA) 0.39], while simultaneously flowing 35°C artificial saliva over the tongue, so that taste and light stimuli were presented under the same experimental conditions. For the whole nerve, the light was positioned at the anterior tip of the tongue and covered as much of the receptive field as possible. For single units, we positioned the fiber-optic over the circumscribed receptive field as precisely as possible.

We stimulated the tongue with a range of light power (in mW: 0.03, 0.1, 0.3, 1, 2), power irradiance (in mW/mm^2: 0.24, 0.8, 2.4, 8.0, 15.9), and frequency (in Hz: 1, 3, 10) to test neuronal sensitivity and faithfulness to respond (percent follow for single units), respectively. For single units, the taste and light protocols were repeated twice and averaged. Mechanosensory neurons were simply stimulated with the glass probe, light (2 mW), and the probe + light (2 mW).

Behavior

All behavioral two-bottle preference tests were conducted in our custom-built lickometer apparatus, which has been thoroughly described previously (Raymond et al., 2018). Details of training and experimental design for each group are outlined in Table 1. At the time of testing, mice were removed from the home cage and placed within the apparatus. Inside the apparatus, mice had 30 min of free access to the following two bottles: 0.3 M NaCl and H_2O or illuminated H_2O and nonilluminated H_2O. Licking data on both spouts were collected by the apparatus and recorded in the open-source audio program Audacity before being exported to R for analysis as described previously (Raymond et al., 2018). Each trial was repeated on the following day with the bottles reversed to account for any inherent side preference. Though some behavioral research has used deionized H_2O as the solvent for mixing taste solutions, tap H_2O served as the solvent for all taste solutions, as our mice have never had access to deionized H_2O and because switching animals accustomed to tap water to deionized water for experimentation can increase variability under certain conditions (Schnorr and Brookshire, 1965).

The rapid induction of salt appetite in mice

To examine the role of type I TBCs in salt taste, we required a reliable behavioral assay of Na^+ appetite. As such, our next aim was to replicate and expand on previous findings demonstrating the induction of Na^+ appetite by self-administration of the potassium-sparing diuretic amiloride (Caloiero and Lundy, 2004). Where the previous study had been conducted in rats and had used 100 μM amiloride in home cage H_2O in conjunction with a Na^+-deplete diet, we aimed to assess whether

Table 1. Timeline of behavioral training and testing schedule

	Apparatus training[a]					Sodium deplete testing[b]									
Group 1–3	Water off		Water on			Amiloride on									
Day	1[c]	2[c]	3	4	5	6	7	8[d]	9[d]						
Group 1	Apparatus training[a]					Sodium deplete testing[e]							Sodium replete testing			
	Water off		Water on			Amiloride on				Water on			Water on			
Day	1[c]	2[c]	3	4	5	6	7	8[f]	9[f]	10	11	12	13	14	15[f]	16[f]
Group 2	Apparatus training[a]					Sodium replete testing							Sodium deplete testing[e]			
	Water off		Water on			Water on				Water on			Amiloride on			
Day	1[c]	2[c]	3	4	5	6	7	8[f]	9[f]	10	11	12	13	14	15[f]	16[f]

[a]H_2O bottles removed from home cages ~24 h before the start of this phase.
[b]H_2O on home cages replaced on the first day of this phase with amiloride (300 μM), photobleached amiloride, or H_2O, depending on condition (group) assigned.
[c]30 min sessions with H_2O and 0.2 M sucrose.
[d]30 min sessions with H_2O and 0.3 M NaCl.
[e]H_2O on home cages were replaced with amiloride (300 μM) on the first day of this phase.
[f]30 min sessions with H_2O and 10 mW 470 nm light.

amiloride could also be used in WT mice, without altering diet. Additionally, because an inactive analog of amiloride does not exist, we attempted to create an inactive control treatment (negative control) for amiloride by destroying the drug with light (photobleached), since it is recommended on the product sheet to protect amiloride from light.

Naive WT mice were divided evenly into three groups: treatment with standard amiloride ($n = 6$; 3 male and 3 female), treatment with photobleached amiloride ($n = 6$; 3 male and 3 female), or no treatment (control; $n = 6$; 3 male and 3 female). Amiloride was dissolved in H_2O to a concentration of 300 μM. Half of this solution was set aside to be used directly on the home cage (and protected from light), whereas the other half was placed in a clear glass flask and exposed directly to a 40 W incandescent lamp (total exposure time, ~72 h). The two amiloride solutions were then placed in the home-cage water bottles of the mice in the experimental groups.

Approximately 48 h before testing, H_2O bottles were changed on the home cage to H_2O, H_2O + 300 μM amiloride, or H_2O + 300 μM photobleached amiloride. Bottles on home cages containing amiloride were protected from light. Mice continued to have free access to food in their home cage. Once inside the apparatus, mice had 30 min of free access to the following two solutions: 0.3 M NaCl and H_2O. Each trial was repeated on the following day with the bottles reversed to account for any inherent side preference. The protocol was presented at the 2017 Association for Chemoreception Sciences Annual Meeting (Raymond et al., 2017) and was recently validated by others (Lossow et al., 2020a) as a rapid method for inducing Na^+ appetite.

Preference for light in Na^+-depleted mice

GAD65-ChR2-EYFP mice ($n = 16$; 8 male and 8 female) and Ai32 mice ($n = 9$; 5 male and 4 female) were separated into two groups. Mice completed an identical series of trials under deplete and replete conditions, and the order of the two assays was counterbalanced between groups (deplete first–replete second vs replete first–deplete second) to control for order effects. Table 1 outlines the behavioral paradigm for the two assays. The 48 h amiloride treatment (amiloride protected from light) was the same as described above for WT mice. Once inside the chamber, mice had 30 min of free access to two bottles; both contained H_2O, but one was modified with a 1 mm fiber-optic cable (NA 0.5) producing 10 mW of 470 nm light (power irradiance = 3.18 mW/mm^2). The spout was constantly illuminated, so that the anterior tongue was optogenetically stimulated throughout the duration of each lick. Licking data on both spouts were collected by the apparatus and recorded in Audacity before being exported to R for analysis. Within condition, the trial was repeated on the following day with the bottles reversed to account for any inherent side preference. Animals were given 3 d off before the start of the new condition.

Experimental design and analyses

Immunohistochemistry

Fluorescent photomicrographs of the anterior tongue were used for analysis of immunohistochemical labeling. ImageJ was used to process the images for maximum clarity and for cell-counting purposes. Fluorescent cells were counted manually using the Cell Counter plugin for ImageJ, and only cells with nuclei clearly labeled by DAPI were considered for the analysis of coexpression between cell types (Boggs et al., 2016). Identified cells were then marked and determined whether they were labeled with EYFP, NTPDase2, PLCβ2, or CA4, or whether they coexpressed EYFP and NTPDase2, EYFP and PLCβ2, or EYFP and CA4.

Neurophysiology

CT-nerve. The peak of the integrated neural response was detected automatically via Spike2 with a vertical cursor, and the voltage at the peak was subtracted from the mean voltage of the 5 s baseline immediately before each stimulus. Peak responses were calculated for each stimulus by dividing each taste and light response by the average 0.1 M NH_4Cl at the beginning and end of the protocol, as shown previously (Whiddon et al., 2018). Consistent responses (criteria ±15%) to 0.1 M NH_4Cl at the beginning and end of the protocol were indicators of nerve integrity and recording stability.

Single units. Spike templates were created from the filtered neural data using spike amplitude (criteria > 3:1 stimulus-to-noise ratio) and waveform shape. Spontaneous firing rates for each neuron was calculated as the average number of spike per second immediately before stimulus onset. An aggregate of the spontaneous firing rates (calculated as the average of spontaneous activity before taste application) was used as the baseline for each neuron, so that response magnitudes to light stimulation could be more directly compared with taste stimulation. Most mechanosensory units had no spontaneous activity, but 1 s of data before mechanosensory stimulation was taken as a measurement of spontaneous activity. Because mechanosensory stimulation was brief, we analyzed spikes for 1 s during stimulation. For gustatory neurons, we calculated the average number of spikes/s over a 10 s period immediately before each taste stimulus. The ratio of response frequency to taste stimuli was calculated as the difference between the baseline of the neuron and the average number of spikes per second occurring during 10 s of stimulation. Neurons were categorized based on their responses to the six taste stimuli (0.2 M sucrose, 0.1 M NaCl, 0.01 M citric acid, 0.01 M QHCl, 0.1 M NH_4Cl, 0.1 M NaCl + benzamil) by a hierarchal cluster analysis using Pearson's product-moment correlation coefficient ($1 - r$) and the average-linking method between subjects (Statistica, StatSoft; Breza et al., 2010; Breza and Contreras, 2012a,b)

Responses to five taste stimuli were used to determine the breadth of tuning (H) for each neuron (Geran and Travers, 2006; Breza et al., 2010; Breza and Contreras, 2012b), calculated as $H = -K \sum p_i \log p_i$, where K is a scaling constant (1.431 for five stimuli; 0.2 M sucrose, 0.1 M NaCl, 0.01 M citric acid, 0.01 M QHCl, and 0.1 M NH_4Cl) and p_i is the proportion of the response to individual stimuli to which the neuron responded against the total responses to all stimuli (Smith and Travers, 1979). Breadth of tuning indicates how narrowly or broadly tuned a neuron is, and H values provide a quantitative measure of breadth of tuning. H values range from 0 to 1, with a value of 0 representing neurons that only

responded to one stimulus and a value of 1 representing neurons that responded equally to all stimuli. Lower H values correspond to more narrowly tuned neurons, while H values closer to 1 correspond to more broadly tuned neurons. The noise-to-signal ratio (N/S) was also calculated for all neurons, as the product of the response to the second-best stimulus and the reciprocal of the response to the best stimulus (N/S = second best stimulus × 1/best stimulus) and compared with H values (Spector and Travers, 2005; Breza and Contreras, 2012a,b).

For single units, responses to light stimulation were analyzed for the frequency of evoked action potentials (in spikes/s), response latency, and ability to follow light (percent follow). The number of light pulses were balanced for each parameter (10 pulses for each frequency and power), so that error associated with latency was not because of differences in the number of samples. As with taste stimulation, response frequency was calculated as the difference between the baseline of the neuron and the average number of spikes per second occurring during the stimulation period.

Response latencies were calculated automatically in Spike2 by using the light-onset marker and automatic detection of a spike via vertical cursors. We used an empirically derived cutoff for measurement of latency, where latencies >65 ms were considered a "failed" response and were excluded from analysis. This was based on several S neurons, which were clearly responsive to light but had long latencies (up to 65 ms). Jitter, the variability in neural firing, was calculated by obtaining the SD of latencies for each neuron and then was averaged within a neuron type. The ability of neurons to follow light (percent follow) was determined by using the data obtained from analyzing its response latency.

Behavior. Details on data processing have been described previously (Raymond et al., 2018). Briefly, raw data recordings were exported from Audacity as .CSV files (Spike2) and imported into R (an open-source statistical software package). These data were processed via a custom script written to accompany the apparatus, calculating the total lick counts on both spouts and filtering out double contacts, as described previously (Raymond et al., 2018). Once this information had been computed, Statistica was used to conduct statistical analysis of the data.

Statistical analyses

For CT nerve recordings, responses to taste and light stimuli in GAD65-ChR2-EYFP and Ai32 mice were compared via mixed ANOVA (strain × stimulus). For single units, baseline responses for each neuron type were compared via one-way ANOVA. Responses to taste and light stimulation in single units (spike rate to light power, spike rate to light-pulse frequency, percent follow of spikes, spike latency, and jitter) were analyzed by mixed ANOVAs to compare main effects and interactions within and between neuron types. Subsequent one-way repeated-measures (RM) ANOVAs were used to compare latency and jitter collapsed across neuron type.

For behavioral tests, preference scores and lick rates for WT, GAD65-ChR2-EYFP, and Ai32 mice were compared using appropriate ANOVAs. For WT mice, differences in preference scores for Na^+-depletion state (amiloride vs photobleached amiloride vs control) in male and female mice were compared with a two-way ANOVA (sex × condition). Lick rates in response to 0.3 M NaCl and H_2O in WT mice were analyzed with a mixed ANOVA (stimulus × condition). Differences in preference scores to illuminated H_2O and H_2O by male and female GAD65-ChR2-EYFP and Ai32 mice under Na^+-deplete and Na^+-replete states (and the order of depletion state) were compared using mixed ANOVAs (sex × strain × condition × order). Lick rates in response to illuminated H_2O and H_2O by GAD65-ChR2-EYFP and Ai32 mice in Na^+-deplete and Na^+-replete states were compared via mixed ANOVAs (strain × condition × stimulus). Preference scores of WT mice to 0.3 M NaCl and H_2O and GAD65-ChR2-EYFP mice to illuminated H_2O and H_2O under Na^+-deplete and Na^+-replete conditions were compared by a two-way ANOVA (strain × condition). Lick rates of WT mice to 0.3 M NaCl and H_2O and GAD65-ChR2-EYFP mice to illuminated H_2O and H_2O under Na^+-deplete and Na^+-replete conditions were compared by a mixed ANOVA (strain × condition × stimulus).

Contrast tests were used to understand main effects and interactions. Cohen's d [$d = (\bar{x}_1 + \bar{x}_2)/SD_{pooled}$] was used to indicate the magnitude of the effect for pairwise comparisons. By convention, effect sizes (d) ≤ 0.2 were considered small, whereas 0.5 were considered medium, and ≥0.8 were considered large (Cohen, 1992). Partial η^2 ($\eta^2_{partial} = SS_{effect}/SS_{effect} + SS_{error}$) was used to indicate the magnitude of the effect size from ANOVAs and contrast tests with multiple levels. By convention, effect sizes of $\eta^2_{partial} \leq 0.01$ were considered small, whereas those equal to 0.06 were considered medium, and ≥0.14 were considered large (Cohen, 1988). Criteria for statistically significant effects were set at $p < 0.05$. For transparency, exact F and p values are reported unless values were $<1 \times 10^{-10}$. To correct for multiple comparisons within each ANOVA, we applied the Benjamini–Hochberg linear setup procedure (Benjamini and Hochberg, 1995). The Benjamini–Hochberg critical value = $p < (i/m)Q$, where i is the rank, m is the total number of comparisons, and Q is the false discovery rate. For the procedure, we used a false discovery rate of 5% as it is analogous to the α criterion. Graphic and tabular data are presented as the mean ± SEM.

Results

Immunohistochemistry

The morphology of GAD65-ChR2-EYFP cells were consistent with those described previously as type I cells; having a "whispy" and irregular appearance—quite unlike PLCβ2 and CA4 cells, which had obvious soma and elongated processes. Results from histology experiments, shown in Figure 1, are from 13 GAD65-ChR2-EYFP mice (7 male and 6 female). Shown in Figure 1 are examples of native GA65-ChR2-EYFP-expressing taste cells and immunohistochemical labeling of putative markers for type I (NTPDase2; Fig. 1*A*), type II (PLCβ2; Fig. 1*B*), and type III (CA4; Fig. 1*C*) cells, at 100×, stained with DAPI (for nuclear staining), and a Venn diagram of coexpression. DAPI is a reliable marker for cell identification (Boggs et al., 2016). Consistent with the literature, we observed extensive coexpression of NTPDase2 in the membrane of GAD65$^+$ cells (Fig. 1*A*). EYFP was not coexpressed in PLCβ2 or CA4 cells. GAD65-ChR2-EYFP cells wrapped closely around PLCβ2- and CA4-expressing cells (Fig. 1*B*,*C*). Two Ai32 mice (1 male and 1 female) were used to validate that EYFP was not expressed in NTPDase2 cells. We observed no FITC fluorescence in Ai32 mice, confirming that the expression of EYFP occurred only in offspring of GAD65cre × Ai32 mice (data not shown).

Neurophysiology

CT nerve

Figure 2*A* shows typical raw CT nerve responses of a GAD65-ChR2-EYFP and an Ai32 mouse, and the average of 5 GAD65-ChR2-EYFP mice (3 male and 2 female) and 4 Ai32 mice (2 male and 2 female; Fig. 2*A*). As expected, a mixed ANOVA showed that there were significant differences in CT responses between mouse strain ($F_{(1,7)} = 5.96$, $p = 0.045$, $\eta^2_{partial} = 0.46$), stimulus ($F_{(18,126)} = 14.61$, $p < 1 \times 10^{-10}$, $\eta^2_{partial} = 0.68$), and a strain × stimulus interaction ($F_{(18,126)} = 8.55$, $p < 1 \times 10^{-10}$, $\eta^2_{partial} = 0.55$). Contrast tests showed that responses to the four basic taste stimuli between transgenic mouse strains were not significantly different ($F_{(1,7)} = 0.35$, $p = 0.573$, $\eta^2_{partial} = 0.05$), but responses to light were significantly different between animal strains. Specifically, responses to light stimulation across the intensity range (0.03–2 mW) were significantly greater in GAD65-ChR2-EYFP mice compared with Ai32 mice at 1 Hz ($F_{(1,7)} = 11.24$, $p = 0.012$, $\eta^2_{partial} = 0.62$), 3 Hz ($F_{(1,7)} = 7.31$, $p = 0.030$, $\eta^2_{partial} = 0.51$), and 10 Hz ($F_{(1,7)} = 7.87$, $p = 0.030$, $\eta^2_{partial} = 0.53$). Within the GAD65-ChR2-EYFP mice, contrast tests showed that nerve responses to light across the intensity range (0.03–2 mW)

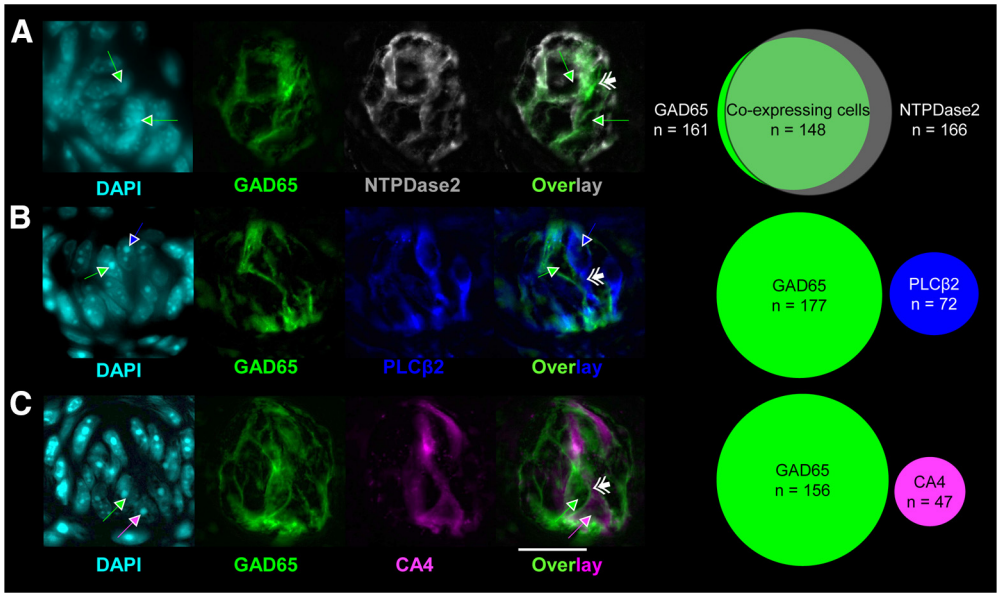

Figure 1. GAD65 is exclusively expressed in putative type I cells in fungiform papillae. ***A–C***, Photomicrographs of native EYFP (green) expression in fungiform papillae immunohistochemically labeled for NTPDase2 (***A***; gray), PLCβ2 (***B***; blue), and CA4 (***C***; magenta). The relative degree of coexpression for each of the proteins is shown in Venn diagrams. DAPI is shown in cyan. Single arrows indicate the location of nuclei and are color coded to indicate whether it was associated with EYFP- (green), PLCβ2- (blue), or CA4- (magenta) expressing cells. Double arrows indicate taste cell membranes. A good example of the glial-like appearance of GAD65$^+$ cells is shown in the EYFP-CA4 overlay. As shown in ***C*** (overlay) the CA4 cell is essentially "hugged" by two adjacent GAD65$^+$ cells. All images were taken with a 100× oil-immersion microscope. Scale bar: (in ***C***) ***A–C***, 20 μm.

increased from 1 to 3 Hz ($F_{(1,7)} = 11.23$, $p = 0.012$, $\eta^2_{partial} = 0.62$) and from 3 to 10 Hz ($F_{(1,7)} = 15.73$, $p = 0.005$, $\eta^2_{partial} = 0.69$).

Within GAD65-ChR2-EYFP-expressing mice, contrast tests showed that nerve responses to 0.1 M NaCl were not significantly different from those to 0.3 mW at 10 Hz ($F_{(1,7)} = 0.47$, $p = 0.516$, $d = 0.1$), or to 1 mW at 10 Hz ($F_{(1,7)} = 1.53$, $p = 0.256$, $d = 0.3$). This was of interest to us, since we wanted to identify a range where NaCl and light were isointense at a frequency similar to the maximum lick rate (8–9 Hz) in C57BL/6J mice (Glatt et al., 2016). Importantly, while whole-nerve recording provides information on the relative effectiveness of chemical and light stimulation of TBCs to generate neural activity, it does not reveal anything about which neuron types were responsive. After applying the Benjamini–Hochberg procedure to adjust for multiple comparisons, p values < 0.031 were considered significant. All p values that were significant before the adjustment remained significant.

Single units

GAD65-ChR2-EYFP mice ($n = 37$; 18 male and 19 female) were used to record 103 neurons (50 gustatory and 53 mechanosensory). On average, gustatory activity from the anterior tongue was encountered 5.8 mm caudal and 1.3 mm lateral to bregma. Mechanosensory activity from the anterior oral cavity was encountered 5.7 mm caudal and 1.4 mm lateral to bregma. These coordinates and the differences in physiology (mechanosensory versus gustatory) are consistent with previously published data in mice (Breza and Travers, 2016).

Additionally, we recorded from 13 neurons (2 mechanosensory and 11 gustatory) in three Ai32 mice (two male and one female). None of the mechanosensory units from GAD65-ChR2-EYFP or Ai32 mice were responsive to light, and light had no effect on mechanosensory activity (mechanosensory + light). Furthermore, consistent with the CT-nerve recordings in Ai32 mice, gustatory neurons in the NTS of Ai32 mice were unresponsive to light. Therefore, control data for the mechanosensory neurons from GAD65-ChR2-EYFP and Ai32 mice and taste responses from Ai32 mice were not examined any further.

Overall response characteristics of gustatory neurons to taste stimuli

Based on spike rates in response to taste stimuli, individual gustatory neurons were grouped according to their stimulus–response profile. Gustatory neurons from GAD65-ChR2-EYFP mice ($n = 50$) were categorized into distinct groups via hierarchical cluster analysis, shown in the dendrogram (Fig. 3*A*). Also shown in Figure 3*B* are the response profiles of each neuron, grouped according to the cluster analysis (four groups/types in the present study: S, SQ, N, and A) and arranged within group/neuron type by the gustatory stimulus that evoked the greatest response in descending order. The response profiles of neuron types that we encountered were remarkably consistent with those of other studies of the mouse NTS (Lemon and Margolskee, 2009; Wilson et al., 2012; Kalyanasundar et al., 2020) and rat geniculate ganglion (Lundy and Contreras, 1999; Breza et al., 2006, 2007, 2010; Breza and Contreras, 2012a,b), despite some differences in solution concentrations and stimulus delivery.

Figure 4 shows an example of a N neuron responding robustly to NaCl through a benzamil-sensitive mechanism. The N neuron was only weakly responsive to an equimolar concentration of NH_4Cl. Figure 4 also shows an A neuron that responded robustly to NH_4Cl. The A neuron also responded well to an equimolar concentration of NaCl, albeit through a benzamil-insensitive mechanism.

A one-way ANOVA revealed no significant differences in baseline activity between neuron types ($F_{(3,46)} = 0.62$, $p = 0.605$, $\eta^2_{partial} = 0.04$). The overall spontaneous firing rate for all 50 gustatory neurons in the NTS was 2.3 spikes/s. As expected, however, a mixed ANOVA showed that there was a significant main effect of taste stimulus ($F_{(5,230)} = 11.84$, $p = 3.4 \times 10^{-10}$, $\eta^2_{partial} = 0.21$) and a neuron type × taste stimulus interaction ($F_{(15,230)} =$

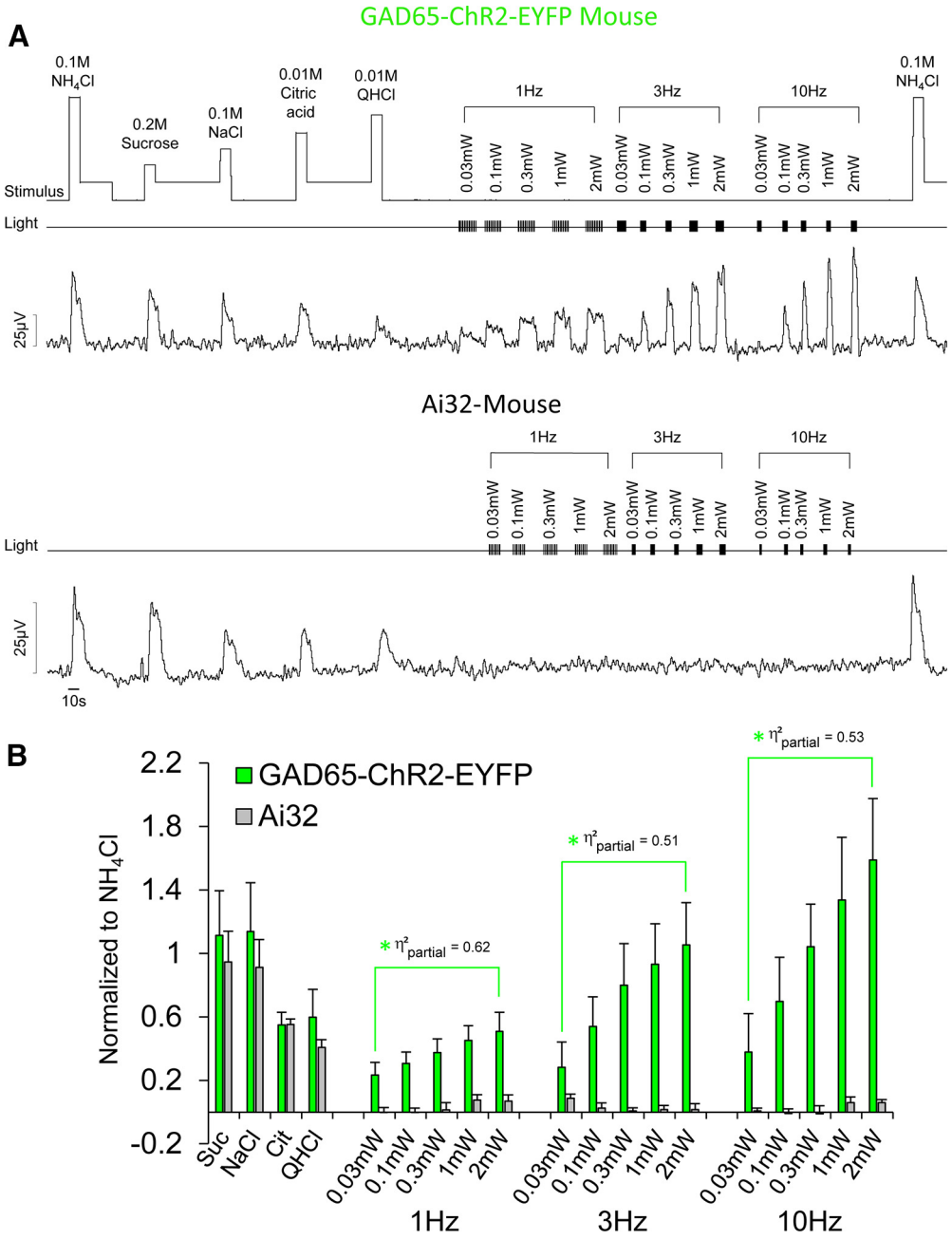

Figure 2. Optogenetic stimulation of type I GAD65$^+$ fungiform TBCs increases CT nerve activity in a dose-dependent manner. ***A***, ***B***, Raw electrophysiological traces from the CT nerve (***A***) of a mouse expressing ChR2 in GAD65$^+$-EYFP TBCs (top), a control Ai32 mouse (middle), which does not express ChR2 (or EYFP), and average responses (***B***) of both mouse strains. A change in rinse to stimulus presentation was indicated by square waves on the "stimulus" channel. Presentation of light pulses are shown by TTL trigger lines on the "light" channel. As shown, responses to taste stimuli representing sweet, salty, sour, and bitter were not significantly different in transgenic mice expressing ChR2-EYFP in GAD65$^+$ cells and Ai32 mice. Nerve activity in GAD65-ChR2-EYFP mice significantly increased with increasing intensity at 1, 3, and 10 Hz, whereas light had no impact on nerve activity in Ai32 mice. The green asterisk and brackets indicate responses significantly different (following Benjamini–Hochberg adjustment) from Ai32 mice. Effect sizes for each contrast test ($\eta^2_{partial}$) are labeled next to each significant comparison.

22.14, $p < 1 \times 10^{-10}$, $\eta^2_{partial} = 0.59$). Contrast tests, $\eta^2_{partial}$, and d were used for specific comparisons tested within each ANOVA within and between neuron types.

S neurons

Figure 5 shows the average 10 s net responses to each taste stimulus. As shown, S neurons responded robustly to sucrose (17.1 spikes/s above baseline), moderately to NH_4Cl, and weakly to other taste stimuli. Responses to sucrose were significantly greater than responses to all other stimuli ($F_{(1,46)} = 105.28$, $p < 1 \times 10^{-10}$, $\eta^2_{partial} = 0.70$). As expected, responses to sucrose in S neurons were not significantly different from sucrose responses in SQ neurons ($F_{(1,46)} = 1.76$, $p = 0.191$, $d = 0.6$), but they were significantly different from sucrose responses in N and A neurons ($F_{(1,46)} = 45.52$, $p = 2.2 \times 10^{-8}$, $\eta^2_{partial} = 0.50$).

S neurons responded second best to NH_4Cl with 5.7 spikes/s above baseline. One neuron, labeled as neuron 8 in Figure 3, responded best to NH_4Cl and second best to sucrose. Not all S neurons, however, were highly responsive to NH_4Cl, as illustrated in Figure 3. This side-band response to NH_4Cl was significantly greater than responses to all other side-band responses within neuron type ($F_{(1,46)} = 7.27$, $p = 0.010$, $\eta^2_{partial} = 0.14$). Interestingly,

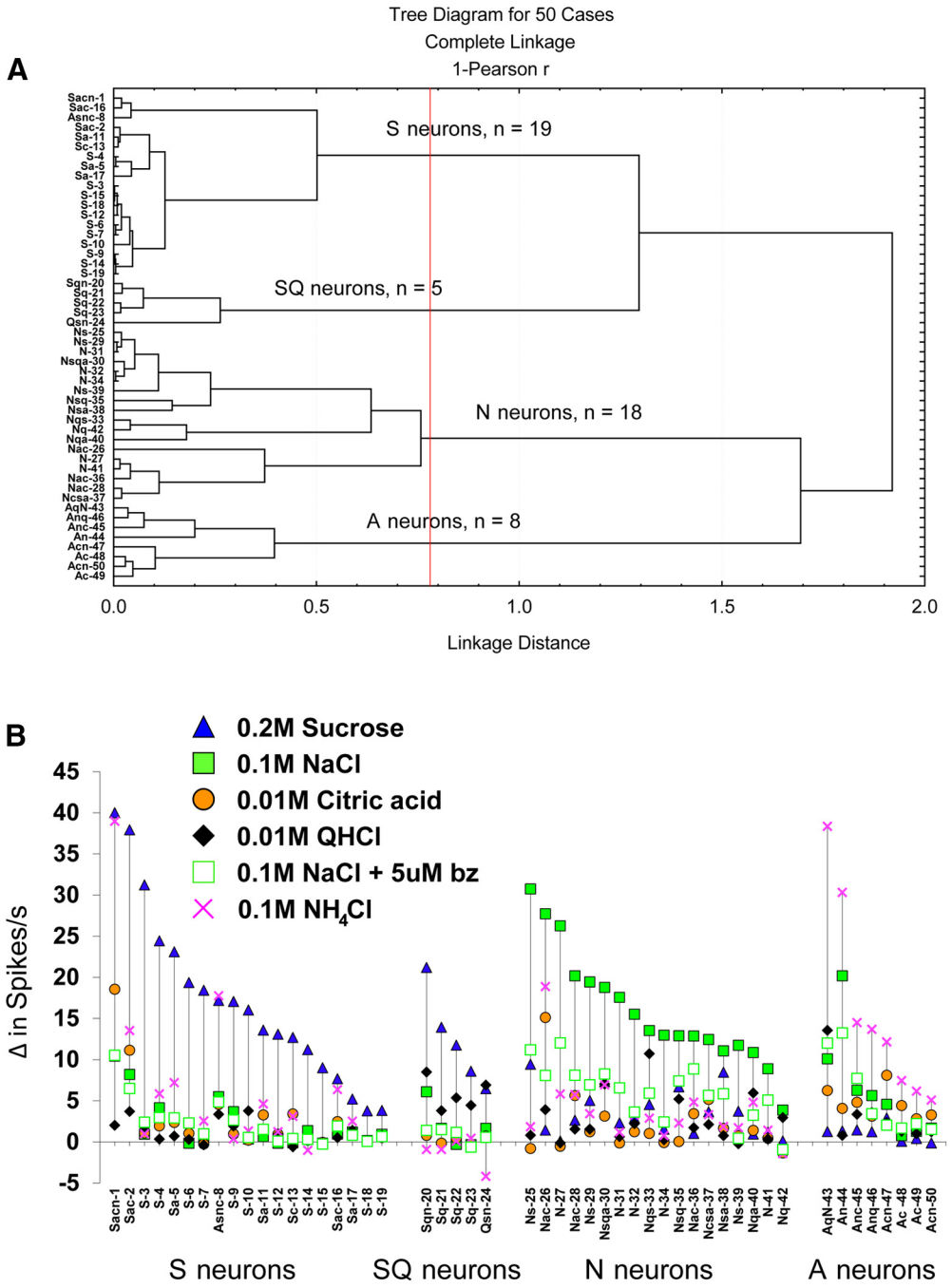

Figure 3. Gustatory neurons grouped by stimulus response profile. ***A***, Dendrogram showing the results of the hierarchical cluster analysis. Next to each neuron is the capital letter indicating the taste stimulus (S, 0.2 M sucrose; N, 0.1 M NaCl; C, 0.01 M citric acid; Q, 0.01 M QHCl; A, 0.1 M NH_4Cl) that evoked the best response. Subsequent lower case letters are responses that were ≥25% of the best response. The vertical red line indicates where the scree plot showed an abrupt deflection, separating neurons into four groups. ***B***, Response profiles of all 50 gustatory neurons grouped according to the cluster analysis and arranged within groups by the best response in descending order (left to right). On the figure, benzamil is abbreviated as "bz." Note that for clarity the neuron number and letters indicating its response characteristics are shown in the dendrogram and graph.

although NH_4Cl responses in S neurons were significantly different from other side-band responses, they were not significantly different from NH_4Cl responses in SQ neurons ($F_{(1,46)} = 2.87$, $p = 0.097$, $d = 1.0$), despite having a large effect size.

SQ neurons

SQ neurons were distinct from S neurons based on the cluster analysis, which is consistent with rNTS reports (Lemon and Margolskee, 2009; Wilson et al., 2012). The average response to sucrose was 12.4 spikes/s above baseline (Fig. 5). Within the group, their response to sucrose was greater than all other taste stimuli ($F_{(1,46)} = 16.12$, $p = 0.0002$, $\eta^2_{partial} = 0.26$). As expected, sucrose responses in SQ neurons were significantly greater than those from N and A neurons ($F_{(1,46)} = 8.49$, $p = 0.006$, $\eta^2_{partial} = 0.16$).

Neurons within the SQ cluster had a side-band response to QHCl that was 5.8 spikes/s above baseline, and, unlike S neurons, those in the SQ cluster were unresponsive to NH_4Cl (Fig. 5). One neuron, labeled as neuron 24 in Figure 3, responded best to QHCl and second best to sucrose. Within the group, responses to QHCl were greater than responses to all other side-band taste

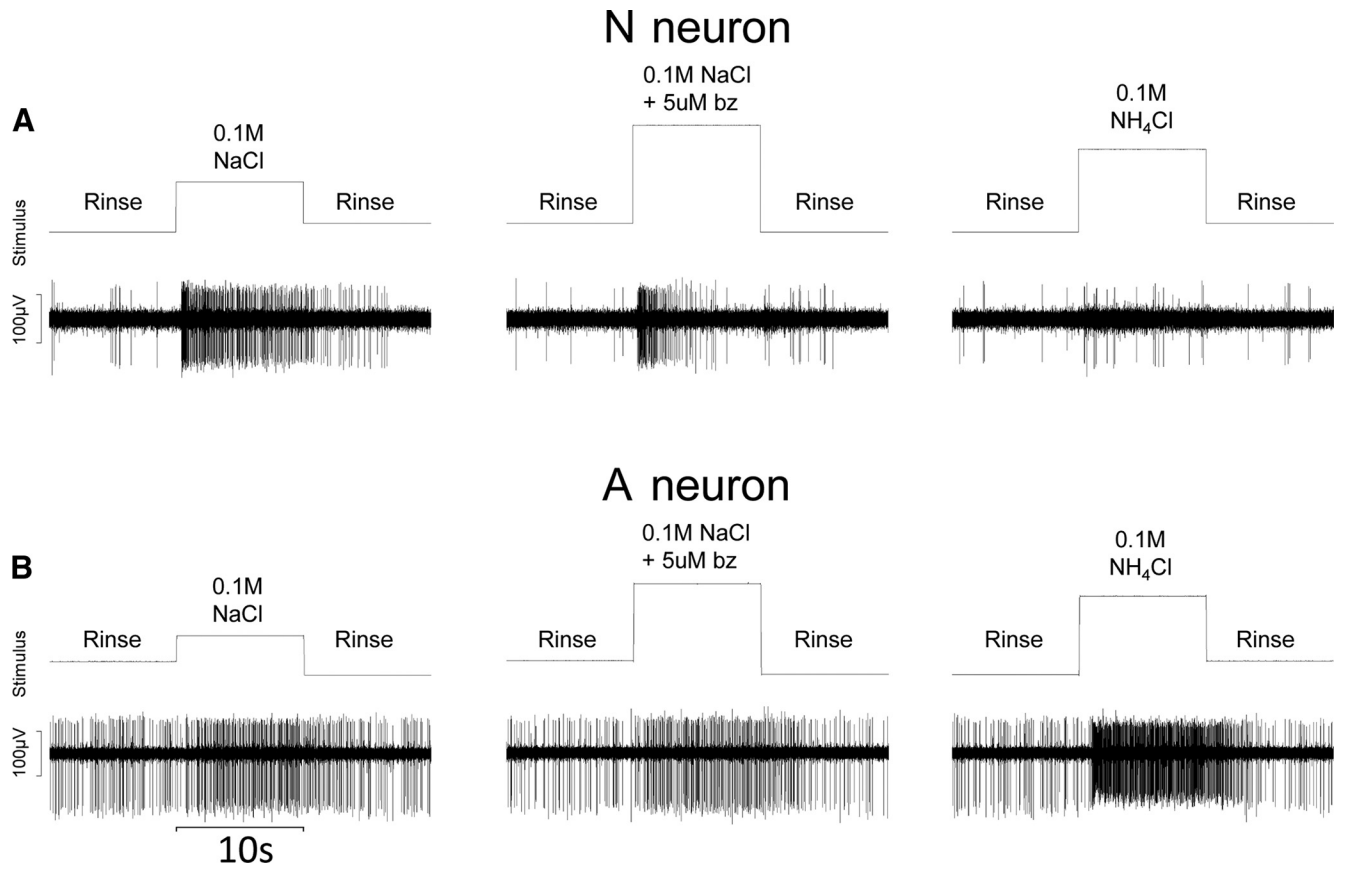

Figure 4. N neurons and A neurons use different receptor mechanisms. ***A***, ***B***, Raw electrophysiological traces from an N neuron (***A***) and from an A neuron (***B***) in response to 0.1 M NaCl, 0.1 M NaCl + 5 μM benzamil (bz), and 0.1 M NH_4Cl. Change in rinse to stimulus presentation was indicated by square waves on the "stimulus" channel. As shown, neural activity in the N neuron was dramatically reduced in the presence of benzamil and was weakly responsive to NH_4Cl, whereas the A neuron was unaffected by benzamil and responded robustly to NH_4Cl.

stimuli ($F_{(1,46)} = 7.48$, $p = 0.009$, $\eta^2_{partial} = 0.14$). Responses to QHCl in SQ neurons were significantly greater than QHCl responses in S neurons ($F_{(1,46)} = 12.23$, $p = 0.001$, $d = 2.8$).

N neurons

N neurons were the only group that responded vigorously to NaCl (net increase, 16.0 spikes/s; Fig. 5). NaCl responses were significantly greater than those to all other stimuli ($F_{(1,46)} = 149.21$, $p < 1 \times 10^{-10}$, $\eta^2_{partial} = 0.76$). As shown in Figures 4 and 5, benzamil significantly reduced NaCl responses by 62% ($F_{(1,46)} = 149.21$, $p < 1 \times 10^{-10}$, $d = 1.8$). Benzamil reduced NaCl responses to the same level as side-band taste responses ($F_{(1,46)} = 167.42$, $p = 0.875$, $\eta^2_{partial} = 0.0005$). Between neuron types, NaCl responses in N neurons were significantly greater than NaCl responses in S, SQ, and A neurons ($F_{(1,46)} = 57.53$, $p = 1.2 \times 10^{-9}$, $\eta^2_{partial} = 0.56$). The addition of benzamil to NaCl disrupted NaCl discrimination between N and A neurons ($F_{(1,46)} = 0.175$, $p = 0.678$, $d = 0.1$).

A neurons

A neurons were the only group that responded vigorously to NH_4Cl (net response, 16.0 spikes/s; Fig. 5). Responses to NH_4Cl were significantly greater than those to all other stimuli ($F_{(1,46)} = 33.37$, $p = 6.3 \times 10^{-7}$, $\eta^2_{partial} = 0.42$). Only one neuron in the A cluster, labeled as neuron 44 in Figure 3, was strongly attenuated by benzamil (NaCl response was reduced by >50%). However, this had no overall effect on the average net responses (Fig. 5), as NaCl and NaCl + benzamil were not statistically different ($F_{(1,46)} = 0.55$, $p = 0.464$, $d = 0.1$). As expected, NH_4Cl responses in A neurons were significantly greater than NH_4Cl responses in S, SQ, and N neurons ($F_{(1,46)} = 17.12$, $p = 0.0002$, $\eta^2_{partial} = 0.27$).

After applying the Benjamini–Hochberg procedure to adjust for multiple comparisons, p values <0.035 were considered significant. All p values that were significant before the adjustment remained significant.

Response characteristics of gustatory neurons to light evoked activity in GAD65$^+$ TBCs—effects of power on spike rate and percent follow

Differences in frequency parameters were used to test the faithfulness of light-evoked responses in gustatory neuron types. Overall and consistent with the hypothesis, N neurons were the most sensitive to light across a wide range of power and responded most faithfully to high-frequency light stimulation. They were the only neuron type that could follow light pulses 90% of the time, beginning at medium intensity and faithfully represented at 10 Hz.

Figure 6*A* shows an example of an N neuron increasing spike rate with increasing power and following light pulses faithfully at 10 Hz. Figure 6*B* shows average response frequencies and percent follow to light across the range of power and frequency. At 1 Hz, mixed ANOVAs showed that there were main effects of power ($F_{(4,152)} = 9.55$, $p = 1 \times 10^{-6}$, $\eta^2_{partial} = 0.200$ and of neuron type ($F_{(3,38)} = 10.39$, $p = 0.00004$, $\eta^2_{partial} = 0.45$) on spike rates. There were also main effects of power ($F_{(4,152)} = 48.62$, $p < 1 \times 10^{-10}$, $\eta^2_{partial} = 0.56$) and neuron type ($F_{(3,38)} = 4.61$, $p = 0.008$, $\eta^2_{partial} = 0.27$), and a power × neuron type interaction ($F_{(12,152)} = 2.60$, $p = 0.004$, $\eta^2_{partial} = 0.17$) on percent follow.

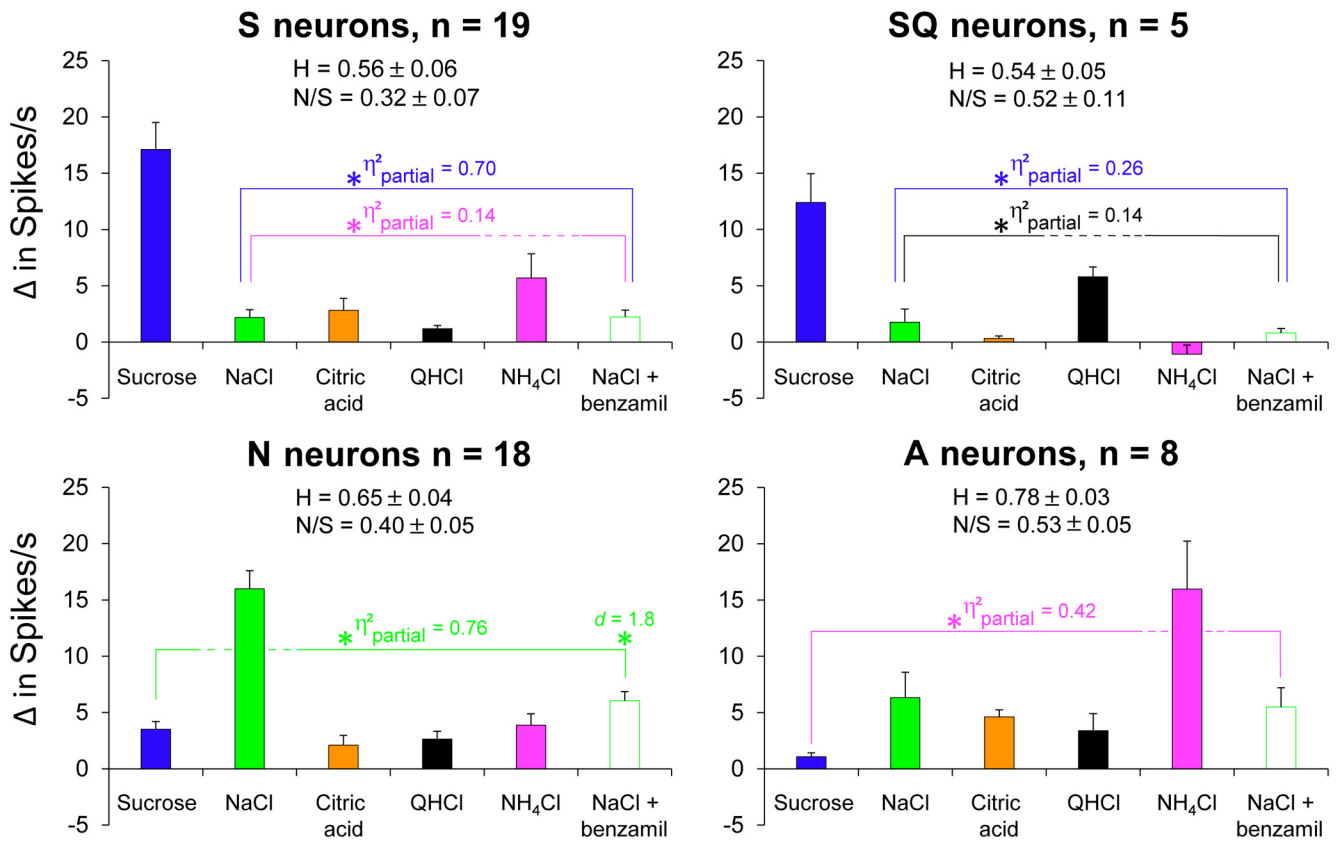

Figure 5. Gustatory neurons respond differentially to taste stimuli. Average responses of gustatory neuron types to taste stimuli. Asterisks (significantly different following Benjamini–Hochberg adjustment), brackets, and effect sizes ($\eta^2_{partial}$ or *d*) are color coordinated to reflect significant differences to taste stimuli within subjects. Blue brackets encompass responses to taste stimuli different from sucrose; green brackets encompass responses to taste stimuli different from NaCl; black brackets encompass responses to taste stimuli different from QHCl; magenta brackets encompass responses to taste stimuli different from NH_4Cl. The breadth of tuning and N/S ratios are shown for each neuron type.

Spike rates of N neurons were three to four times greater in response to light than those from S neurons and were significantly different across the intensity range ($F_{(1,38)} = 22.58$, $p = 0.00003$, $\eta^2_{partial} = 0.37$). N neurons followed light significantly better than S neurons across the intensity range ($F_{(1,38)} = 12.23$, $p = 0.001$, $\eta^2_{partial} = 0.24$). Spike rates of N neurons in response to light at 1 Hz were 5–21 times greater than those from SQ neurons and were significantly different across the intensity range ($F_{(1,38)} = 16.90$, $p = 0.0002$, $\eta^2_{partial} = 0.31$). N neurons followed light significantly better than SQ neurons across the intensity range ($F_{(1,38)} = 4.73$, $p = 0.036$, $\eta^2_{partial} = 0.11$). Spike rates of N neurons to light at 1 Hz were two times greater than those from A neurons and were significantly different across the intensity range ($F_{(1,38)} = 6.72$, $p = 0.014$, $\eta^2_{partial} = 0.15$). Interestingly, however, the ability to follow light across the intensity range did not differ between N and A neurons ($F_{(1,38)} = 2.70$, $p = 0.109$, $\eta^2_{partial} = 0.07$).

Spike rates of S neurons to light across the intensity range were not significantly different from SQ neurons ($F_{(1,38)} = 1.93$, $p = 0.173$, $\eta^2_{partial} = 0.05$) or A neurons ($F_{(1,38)} = 1.79$, $p = 0.189$, $\eta^2_{partial} = 0.05$). Compared with SQ neurons, A neurons responded to light across the intensity range with significantly higher spike rates ($F_{(1,38)} = 4.68$, $p = 0.037$, $\eta^2_{partial} = 0.11$). The ability for S, SQ, and A neurons to follow light across the intensity range were not significantly different. Specifically, the percent follow was not significantly different between S and SQ neurons ($F_{(1,38)} = 0.03$, $p = 0.862$, $\eta^2_{partial} = 0.0008$), S and A neurons ($F_{(1,38)} = 1.55$, $p = 0.220$, $\eta^2_{partial} = 0.04$), or SQ and A neurons ($F_{(1,38)} = 0.94$, $p = 0.338$, $\eta^2_{partial} = 0.02$).

After applying the Benjamini–Hochberg procedure to adjust for multiple comparisons, p values <0.025 were considered significant for spike rates, whereas p values <0.017 were considered significant for percent follow. Most p values that were significant before the adjustment remained significant. The only exceptions were that spike rates in response to light between SQ and A neurons ($p = 0.037$) and the percent follow between N and SQ neurons ($p = 0.036$) were not significantly different after the adjustment.

At 3 Hz, mixed ANOVAs showed that there were main effects of power ($F_{(4,152)} = 26.45$, $p < 1 \times 10^{-10}$, $\eta^2_{partial} = 0.41$) and of neuron type ($F_{(3,38)} = 7.34$, $p = 0.0005$, $\eta^2_{partial} = 0.37$) on spike rates. There were also main effects of power ($F_{(4,152)} = 46.06$, $p < 1 \times 10^{-10}$, $\eta^2_{partial} = 0.55$) and neuron type ($F_{(3,38)} = 5.07$, $p = 0.005$, $\eta^2_{partial} = 0.29$), and a power × neuron type interaction ($F_{(12,152)} = 2.09$, $p = 0.021$, $\eta^2_{partial} = 0.14$) on percent follow. N neurons were the only group that were capable of following light >90%.

Spike rates of N neurons were two to eight times greater in response to light than those from S neurons and were significantly different across the intensity range ($F_{(1,38)} = 16.08$, $p = 0.0003$, $\eta^2_{partial} = 0.30$). N neurons followed light significantly better than S neurons across the intensity range ($F_{(1,38)} = 12.42$, $p = 0.001$, $\eta^2_{partial} = 0.25$). Spike rates of N neurons at 3 Hz were 3–31 times greater in response to light than those from SQ neurons and were significantly different across the intensity range ($F_{(1,38)} = 11.77$, $p = 0.002$, $\eta^2_{partial} = 0.24$). N neurons also followed light significantly better than SQ neurons across the intensity range ($F_{(1,38)} = 6.35$, $p = 0.016$, $\eta^2_{partial} = 0.14$). Spike rates of N

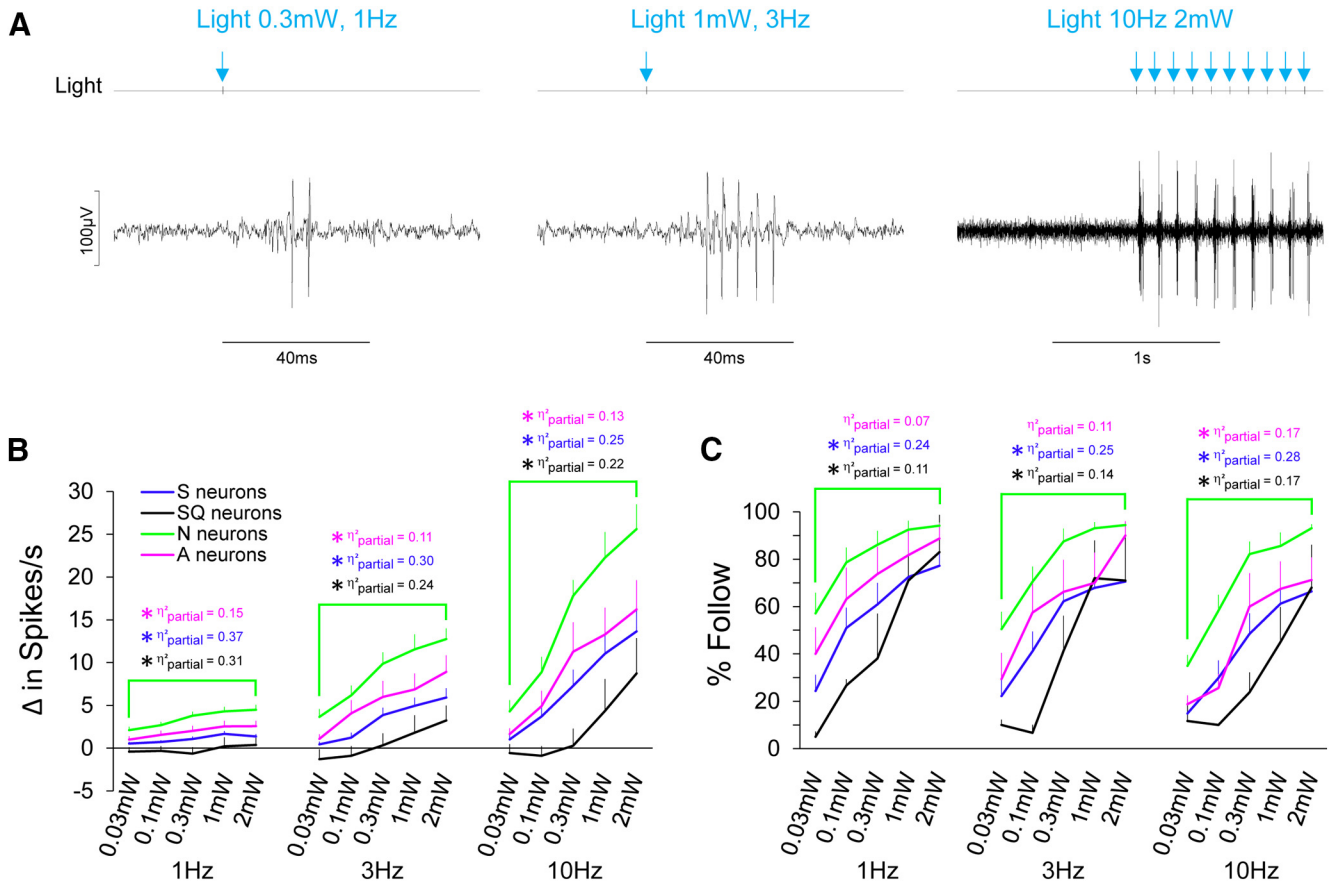

Figure 6. N neurons respond robustly and faithfully to light in a dose-dependent manner. ***A***, Raw electrophysiological traces from an N neuron in response to light pulses at varying intensities and pulse frequencies. Light pulses, by way of TTL trigger are shown on the light channel and also by blue arrows for convenience. ***B***, Average spike per second of gustatory neuron types to optogenetic stimulation of fungiform receptive fields to a range of intensities (0.03–2 mW) at 1, 3, and 10 Hz. ***C***, The ability for gustatory neuron types to follow light pulses across the range of light intensity and pulse frequency are shown. Asterisks are color coordinated to reflect significant differences (following Benjamini–Hochberg adjustment) between neuron groups. The effect size ($\eta^2_{partial}$) of each statistical comparison is also color coordinated. Blue indicates comparisons between N and S neurons; black indicates comparisons between N and SQ neurons; magenta indicates comparisons between N and A neurons.

neurons were 1.4–3.4 times greater in response to light than those from A neurons and were significantly different across the intensity range ($F_{(1,38)} = 4.80$, $p = 0.035$, $\eta^2_{partial} = 0.11$). As with 1 Hz stimulation, there was not a significant difference in the ability for N and A neurons to follow light across the intensity range at 3 Hz ($F_{(1,38)} = 4.07$, $p = 0.051$, $\eta^2_{partial} = 0.11$), though the p value approached significance with a medium-sized effect.

Spike rates and percentages of follow of S, SQ, and A neurons at 3 Hz were not significantly different. Specifically, spike rates in response to light across the intensity range were not significantly different between S and SQ neurons ($F_{(1,38)} = 1.29$, $p = 0.264$, $\eta^2_{partial} = 0.03$), S and A neurons ($F_{(1,38)} = 1.27$, $p = 0.268$, $\eta^2_{partial} = 0.03$), or SQ and A neurons ($F_{(1,38)} = 3.19$, $p = 0.082$, $\eta^2_{partial} = 0.08$). The percent follow across the intensity range at 3 Hz was not significantly different between S and SQ neurons ($F_{(1,38)} = 0.25$, $p = 0.617$, $\eta^2_{partial} = 0.007$), S and A neurons ($F_{(1,38)} = 0.80$, $p = 0.376$, $\eta^2_{partial} = 0.02$), and SQ and A neurons ($F_{(1,38)} = 1.10$, $p = 0.300$, $\eta^2_{partial} = 0.03$). After applying the Benjamini–Hochberg procedure to adjust for multiple comparisons, p values < 0.0250 were considered significant for spike rates and for percentages of follow. Most p values that were significant before the adjustment remained significant. The only exceptions were that spike rates in response to light between N and A neurons ($p = 0.035$) were not significantly different after the adjustment.

At 10 Hz, mixed ANOVAs showed that there were main effects of power ($F_{(4,152)} = 32.69$, $p < 1 \times 10^{-10}$, $\eta^2_{partial} = 0.46$) and of neuron type ($F_{(3,38)} = 6.33$, $p = 0.001$, $\eta^2_{partial} = 0.33$) on spike rates. There were also main effects of power ($F_{(4,152)} = 55.22$, $p < 1 \times 10^{-10}$, $\eta^2_{partial} = 0.59$) and neuron type ($F_{(3,38)} = 6.35$, $p = 0.001$, $\eta^2_{partial} = 0.33$) on percent follow. N neurons were the only group that were capable of following light >90%.

Spike rates of N neurons were two to four times greater in response to light than those from S neurons. N neurons responded significantly better than S neurons across the intensity range ($F_{(1,38)} = 12.83$, $p = 0.001$, $\eta^2_{partial} = 0.25$). N neurons also followed light significantly better than S neurons across the intensity range ($F_{(1,38)} = 14.46$, $p = 0.0005$, $\eta^2_{partial} = 0.28$). Spike rates of N neurons were 3–64 times greater in response to light than those from SQ neurons and were significantly different across the intensity range ($F_{(1,38)} = 10.60$, $p = 0.002$, $\eta^2_{partial} = 0.22$). N neurons also followed light significantly better than SQ neurons across the intensity range ($F_{(1,38)} = 7.65$, $p = 0.009$, $\eta^2_{partial} = 0.17$). Spike rates of N neurons were 1.6–2.6 times greater in response to light than those from A neurons across the intensity range ($F_{(1,38)} = 5.87$, $p = 0.020$, $\eta^2_{partial} = 0.13$). N neurons also followed light significantly better than A neurons across the intensity range ($F_{(1,38)} = 7.98$, $p = 0.008$, $\eta^2_{partial} = 0.17$).

Spike rates and the percent follow of S, SQ, and A neurons were not significantly different from one another at 10 Hz. Specifically, spike rates in response to light across the intensity range were not significantly different between S and SQ neurons ($F_{(1,38)} = 1.45$, $p = 0.237$, $\eta^2_{partial} = 0.37$), S and A neurons ($F_{(1,38)} = 0.30$, $p = 0.590$, $\eta^2_{partial} = 0.008$), or SQ and A neurons ($F_{(1,38)} = 2.18$, $p = 0.148$, $\eta^2_{partial} = 0.05$). The percent follow across the intensity

Table 2. Effects of light power (in mW) on response latency to light at 1, 3, and 10 Hz across all 50 gustatory neurons

	Power					Jitter
Frequency	0.03 mW	0.1 mW	0.3 mW	1 mW	2 mW	2 mW
1 Hz	33.6 ± 1.3	32.5 ± 1.5	26.1 ± 1.4*	23.6 ± 1.2*	23.3 ± 1.2	4.9
3 Hz	35.9 ± 1.4	32.7 ± 1.1*	28.2 ± 1.3*	26.3 ± 1.3*	23.8 ± 0.9*	4.9
10 Hz	36.9 ± 1.5	33.8 ± 1.5	30.7 ± 1.5	28.8 ± 1.5*	28.5 ± 1.3	6.7†

*Significant differences from preceding power within frequency.
†Significant differences in jitter (at 2 mW) between pulse frequencies.

range at 10 Hz was not significantly different between S and SQ neurons ($F_{(1,38)} = 0.35$, $p = 0.558$, $\eta^2_{partial} = 0.009$), S and A neurons ($F_{(1,38)} = 0.11$, $p = 0.745$, $\eta^2_{partial} = 0.003$), or SQ and A neurons ($F_{(1,38)} = 0.59$, $p = 0.449$, $\eta^2_{partial} = 0.02$). After applying the Benjamini–Hochberg procedure to adjust for multiple comparisons, p values <0.0250 were considered significant for spike rates and for percentages of follow. All p values that were significant before the adjustment remained significant.

Response characteristics of gustatory neurons to optogenetic stimulation of GAD65$^+$ TBCs—effects of power on spike latency and jitter

Gustatory neurons had side-band responses to taste stimuli and to light, which could be the result of paracrine signaling within taste buds and/or neuronal convergence. We addressed whether response latencies and jitter in response to light stimulation would provide insight into the synaptic complexity of this circuit. To determine whether spike latency was affected by stimulus intensity, we compared response latencies of 0.03–2 mW. Contrary to our expectations, a mixed ANOVA showed no significant differences in latency between neuron types at 1, 3, or 10 Hz stimulation, so we measured the effect of power on response latency across all 50 neurons. Response latencies to light pulses collapsed across neuron types are shown in Table 2. Though nonsignificant, it is worth noting that average response latencies in N neurons were shorter than those from other neuron types. Response latencies to 2 mW at 1 Hz (999 ms of recovery between pulses and the highest percent follow from all neurons) were as follows: N neurons, 20.8 ± 1.1 ms; S neurons, 23.1 ± 2.2 ms; SQ neurons, 27.8 ± 5.7 ms; A neurons, 26.2 ± 3.2 ms.

At 1 Hz, a one-way RM ANOVA showed a significant main effect of power ($F_{(4,144)} = 26.09$, $p < 1 \times 10^{-10}$, $\eta^2_{partial} = 0.42$) on response latency to light. Response latencies to 0.03 and 0.1 mW did not differ ($F_{(1,36)} = 0.08$, $p = 0.773$, $d = 0.1$), but became significantly shorter as power increased from 0.1 to 0.3 mW ($F_{(1,36)} = 40.26$, $p < 2.5 \times 10^{-7}$, $d = 0.6$) and 0.3 to 1 mW ($F_{(1,36)} = 11.08$, $p = 0.002$, $d = 0.5$). Latencies were not significantly different at 1 and 2 mW ($F_{(1,36)} = 2.0$, $p = 0.166$, $d = 0.1$). After applying the Benjamini–Hochberg procedure to adjust for multiple comparisons, p values <0.025 were considered significant. All p values that were significant before the adjustment remained significant.

At 3 Hz, a one-way RM ANOVA showed a significant main effect of power ($F_{(4,124)} = 30.02$, $p < 1 \times 10^{-10}$, $\eta^2_{partial} = 0.49$) on the response latency to light. Response latencies were significantly shorter as power increased from 0.03 to 0.1 mW ($F_{(1,31)} = 5.80$, $p = 0.022$, $d = 0.5$), from 0.1 to 0.3 mW ($F_{(1,31)} = 13.03$, $p = 0.001$, $d = 0.5$), from 0.3 to 1 mW ($F_{(1,31)} = 7.93$, $p = 0.008$, $d = 0.3$), and from 1 to 2 mW ($F_{(1,31)} = 10.02$, $p = 0.003$, $d = 0.3$). After applying the Benjamini–Hochberg procedure to adjust for multiple comparisons, p values <0.05 were considered significant. All p values that were significant before the adjustment remained significant.

At 10 Hz, a one-way RM ANOVA showed a significant main effect of power ($F_{(4,132)} = 10.06$, $p = 3.9 \times 10^{-7}$, $\eta^2_{partial} = 0.23$) on response latency to light. Response latencies did not differ at 0.03 and 0.1 mW ($F_{(1,33)} = 2.31$, $p = 0.137$, $d = 0.3$), at 0.1 and 0.3 mW ($F_{(1,33)} = 2.07$, $p = 0.160$, $d = 0.3$), and at 1 and 2 mW ($F_{(1,33)} = 0.78$, $p = 0.383$, $d = 0.03$), but became significantly shorter as power increased from 0.3 to 1 mW ($F_{(1,33)} = 6.42$, $p = 0.016$, $d = 0.2$). There was still a significant decrease in response latency with increasing power, as the latency at 0.03 mW was significantly longer than at 0.3 mW ($F_{(1,33)} = 6.31$, $p = 0.017$, $d = 0.6$), and latency at 0.3 mW was significantly longer than that at 2 mW ($F_{(1,33)} = 6.39$, $p = 0.016$, $d = 0.3$). After applying the Benjamini–Hochberg procedure to adjust for multiple comparisons, p values <0.025 were considered significant. All p values that were significant before the adjustment remained significant.

Based on the ability for neurons to follow light, we calculated the jitter at 1, 3, and 10 Hz and 2 mW of power. As with response latencies, a mixed ANOVA showed no clear differences between neuron types, so we measured the effect of pulse frequency on jitter across all 50 neurons. A one-way RM ANOVA showed a significant effect of pulse frequency ($F_{(2,86)} = 8.50$, $p = 0.0004$, $\eta^2_{partial} = 0.17$) on jitter. Jitter was not statistically different at 1 and 3 Hz ($F_{(1,43)} = 1.79$, $p = 0.189$, $d = 0.005$), but at 3 Hz was significantly different from 10 Hz ($F_{(1,43)} = 12.39$, $p = 0.001$, $d = 0.3$). The increased jitter at high-frequency stimulation is consistent with previous observations of polysynaptic pathways (Doyle and Andresen, 2001). After applying the Benjamini–Hochberg procedure to adjust for multiple comparisons, p values <0.025 were considered significant. The p value that was significant before the adjustment remained significant.

Behavior: Na$^+$ depletion via amiloride evokes "NaCl appetite" and "light appetite"

Figure 7 shows the effects of Na$^+$ depletion on preference scores to 0.3 M NaCl versus H_2O, and of total licks to 0.3 M NaCl and H_2O in WT mice. A two-way ANOVA on preference scores showed a significant main effect of amiloride condition on 0.3 M NaCl preference ($F_{(2,12)} = 209.92$, $p < 1 \times 10^{-10}$, $\eta^2_{partial} = 0.97$), but no significant differences in sex ($F_{(1,12)} = 4.21$, $p = 0.063$, $\eta^2_{partial} = 0.26$). Because there was no effect of sex on preferences, we combined these factors for subsequent testing. A contrast test on condition showed no differences between preference scores for amiloride protected from light versus photobleached amiloride ($F_{(1,12)} = 1.69$, $p = 0.218$, $d = 0.5$). Therefore, we combined both amiloride factors into one group. A contrast test showed that Na$^+$ depletion via amiloride treatment resulted in a significant and robust preference for 0.3 M NaCl relative to Na$^+$-replete mice ($F_{(1,12)} = 418.15$, $p = 1.1 \times 10^{-10}$, $d = 10.0$). After applying the Benjamini–Hochberg procedure to adjust for multiple comparisons, p values <0.025 were considered significant. All p values that were significant before the adjustment remained significant.

For total licks, a mixed ANOVA showed significant main effects of stimulus (H_2O and 0.3 M NaCl; $F_{(1,16)} = 32.86$, $p = 0.00003$, $\eta^2_{partial} = 0.67$), amiloride condition ($F_{(1,16)} = 24.21$, $p = 0.0002$, $\eta^2_{partial} = 0.60$), and a stimulus × condition interaction ($F_{(1,16)} = 29.73$, $p = 0.00005$, $\eta^2_{partial} = 0.65$). Contrast tests within subjects showed that Na$^+$-depleted mice licked 0.3 M NaCl significantly more than H_2O ($F_{(1,16)} = 93.83$, $p = 4.3 \times 10^{-8}$, $d = 3.0$), whereas Na$^+$-replete mice showed no differences in lick rates between 0.3 M NaCl and H_2O ($F_{(1,16)} = 0.03$, $p = 0.87$, $d = 0.5$). Contrast tests between subjects showed that lick rates in response to 0.3 M NaCl were higher in Na$^+$-deplete mice compared with Na$^+$-replete mice ($F_{(1,16)} = 26.86$, $p = 0.00009$, $d = 3.0$); whereas lick rates in response to H_2O were not significantly different in Na$^+$-deplete and Na$^+$-replete mice

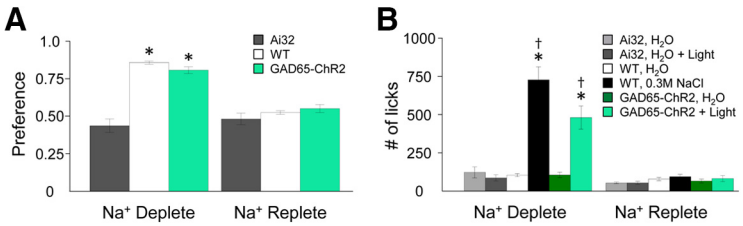

Figure 7. Optogenetic stimulation of type I GAD65$^+$ fungiform TBCs increases behavioral preference and lick rates in Na$^+$-depleted mice. ***A***, ***B***, Preference scores (***A***) and lick rates (***B***) of WT, Ai32, and GAD65-ChR2-EYFP mice are dependent on whether mice were Na$^+$ deplete or Na$^+$ replete. As expected, Na$^+$-depleted mice show a robust preference for 0.3 M NaCl versus H_2O that is similar to preference scores for optogenetic stimulation of GAD65$^+$ TBCs in response to illuminated H_2O versus H_2O. Ai32 mice are indifferent to light while Na$^+$ deplete. All animal strains are indifferent when Na$^+$ replete. Asterisks indicate significant differences (following Benjamini–Hochberg adjustment) between Na$^+$ deplete and Na$^+$ replete conditions. †Differences in lick rates between NaCl or illuminated H_2O and H_2O.

($F_{(1,16)} = 2.68$, $p = 0.121$, $d = 0.8$). After applying the Benjamini–Hochberg procedure to adjust for multiple comparisons, p values <0.025 were considered significant. All p values that were significant before the adjustment remained significant.

To assess the effect of Na$^+$ depletion on optogenetic stimulation of GAD65$^+$ TBCs, we examined behavioral preferences and lick rates in response to illuminated H_2O versus nonilluminated H_2O by GAD-ChR2-EYFP and Ai32 mice under Na$^+$-deplete and Na$^+$-replete conditions. Figure 7 shows the effects of Na$^+$ depletion on preferences and total licks in response to optogenetic stimulation of GAD65-ChR2-EYFP TBCs and Ai32 controls. A mixed ANOVA on preferences showed significant effects of strain ($F_{(1,17)} = 61.24$, $p = 4.9 \times 10^{-7}$, $\eta^2_{partial} = 0.78$) and condition ($F_{(1,17)} = 26.65$, $p = 0.00008$, $\eta^2_{partial} = 0.61$), and a significant strain × condition interaction ($F_{(1,17)} = 40.24$, $p = 7.0 \times 10^{-6}$, $\eta^2_{partial} = 0.70$). Consistent with WT mice, there were no significant main effects of sex ($F_{(1,17)} = 0.61$, $p = 0.447$, $\eta^2_{partial} = 0.03$) or order ($F_{(1,17)} = 0.06$, $p = 0.809$, $\eta^2_{partial} = 0.004$), so subsequent tests were conducted without sex and order as factors. Within subjects, contrast tests showed that when compared with a Na$^+$-replete condition, Na$^+$-depleted GAD65-ChR2-EYFP mice showed significantly greater preferences for illuminated H_2O over nonilluminated H_2O ($F_{(1,17)} = 93.76$, $p = 2.5 \times 10^{-8}$, $d = 2.6$), whereas condition had no effect on preferences in Ai32 mice ($F_{(1,17)} = 0.54$, $p = 0.473$, $d = 0.4$). Contrast tests on the strain × condition interaction showed that while in a Na$^+$-depleted condition, GAD65-ChR2-EYFP mice showed significant preferences for illuminated H_2O versus nonilluminated H_2O compared with Ai32 mice ($F_{(1,17)} = 108.70$, $p = 8.4 \times 10^{-9}$, $d = 3.2$). Importantly, GAD65-ChR2-EYFP and Ai32 mice in a Na$^+$-replete condition showed similar preferences for illuminated H_2O versus nonilluminated H_2O ($F_{(1,17)} = 3.89$, $p = 0.065$, $d = 0.6$). After applying the Benjamini–Hochberg procedure to adjust for multiple comparisons, p values <0.025 were considered significant. All p values that were significant before the adjustment remained significant.

For total licks, a mixed ANOVA showed the main effects of strain ($F_{(1,23)} = 8.72$, $p = 0.007$, $\eta^2_{partial} = 0.28$), stimulus ($F_{(1,23)} = 13.27$, $p = 0.001$, $\eta^2_{partial} = 0.37$), and condition ($F_{(1,23)} = 23.37$, $p = 0.00007$, $\eta^2_{partial} = 0.50$), and significant interactions of stimulus × strain ($F_{(1,23)} = 19.05$, $p = 0.0002$, $\eta^2_{partial} = 0.45$), condition × strain ($F_{(1,23)} = 9.18$, $p = 0.006$, $\eta^2_{partial} = 0.29$), stimulus × condition ($F_{(1,23)} = 10.37$, $p = 0.004$, $\eta^2_{partial} = 0.31$), and stimulus × strain × condition ($F_{(1,23)} = 15.73$, $p = 0.0006$, $\eta^2_{partial} = 0.41$). Within the GAD65-ChR2-EYFP strain, contrast tests showed that lick rates in response to illuminated H_2O were significantly greater than those to nonilluminated H_2O when mice were in a Na$^+$-depleted condition ($F_{(1,23)} = 40.95$, $p = 2 \times 10^{-6}$, $d = 1.7$), but not significantly different when in a Na$^+$-replete condition ($F_{(1,23)} = 3.20$, $p = 0.087$, $d = 0.2$). Contrast tests in Ai32 mice, however, showed no significant differences in lick rates in response to illuminated H_2O versus nonilluminated H_2O regardless of whether they were Na$^+$ deplete ($F_{(1,23)} = 0.22$, $p = 0.647$, $d = 0.4$) or Na$^+$ replete ($F_{(1,23)} = 0.007$, $p = 0.93$, $d = 0.04$).

Contrasts between strain, but within condition and stimulus, showed that lick rates in response to nonilluminated H_2O did not differ in GAD65-ChR2-EYFP and Ai32 mice under Na$^+$-deplete ($F_{(1,23)} = 0.21$, $p = 0.652$, $d = 0.2$) and Na$^+$-replete ($F_{(1,23)} = 0.49$, $p = 0.49$, $d = 0.3$) conditions. However, lick rates in response to illuminated H_2O between strains (ChR2-EYFP and Ai32 mice), were significantly different when Na$^+$ deplete ($F_{(1,23)} = 14.75$, $p = 0.0008$, $d = 1.8$) but not when Na$^+$ replete ($F_{(1,23)} = 0.90$, $p = 0.35$, $d = 0.4$). When examined across conditions but within strain, contrast tests showed that lick rates in response to illuminated H_2O by GAD65-ChR2-EYFP mice were significantly greater when Na$^+$ deplete compared with Na$^+$ replete ($F_{(1,23)} = 43.38$, $p = 1.0 \times 10^{-6}$, $d = 1.8$), whereas lick rates in response to illuminated H_2O by Ai32 mice were not significantly different between Na$^+$-deplete and Na$^+$-replete conditions ($F_{(1,23)} = 0.16$, $p = 0.698$, $d = 0.7$). Collectively, the behavioral data indicate that the major driver of light appetite in transgenic mice was Na$^+$ depletion, and this was only evident in GAD65-ChR2-EYFP mice. After applying the Benjamini–Hochberg procedure to adjust for multiple comparisons, p values <0.015 were considered significant. All p values that were significant before the adjustment remained significant.

We compared preference scores and lick rates of WT mice to 0.3 M NaCl and H_2O and of GAD65-ChR2-EYFP mice to illuminated H_2O and nonilluminated H_2O. A two-way ANOVA on preferences showed no significant differences of strain ($F_{(1,30)} = 0.34$, $p = 0.563$, $\eta^2_{partial} = 0.01$), though, as expected from previous comparisons within WT and GAD65-ChR2-EYFP strains, there was a main effect of Na$^+$ depletion on preference scores ($F_{(1,30)} = 194.44$, $p < 1 \times 10^{-10}$, $\eta^2_{partial} = 0.87$). A mixed ANOVA showed no significant differences in mouse strain ($F_{(1,30)} = 1.05$, $p = 0.315$, $\eta^2_{partial} = 0.03$) for total licks in response to 0.3 M NaCl and H_2O in WT mice, and in response to illuminated H_2O and nonilluminated H_2O in GAD65-ChR2-EYFP mice. As expected, contrast tests showed that there were significant differences in deprivation state ($F_{(1,30)} = 31.47$, $p = 4 \times 10^{-6}$, $\eta^2_{partial} = 0.51$) and stimulus ($F_{(1,30)} = 53.57$, $p = 3.8 \times 10^{-8}$, $\eta^2_{partial} = 0.64$) on licks in response to H_2O versus 0.3 M NaCl or illuminated H_2O versus nonilluminated H_2O. However, there were no significant interactions of strain × deprivation state ($F_{(1,30)} = 2.41$, $p = 0.13$, $\eta^2_{partial} = 0.07$), stimulus × strain ($F_{(1,30)} = 1.74$, $p = 0.197$, $\eta^2_{partial} = 0.06$), or stimulus × strain × deprivation state ($F_{(1,30)} = 2.46$, $p = 0.128$, $\eta^2_{partial} = 0.08$). Thus, there were no significant differences in preference scores or lick rates of Na$^+$-deplete and Na$^+$-replete WT and GAD65-ChR2-EYFP mice in response to H_2O versus 0.3 M NaCl or illuminated H_2O versus nonilluminated H_2O.

Discussion

The role of type I glial-like TBCs in taste physiology and behavior is undefined. Over the past 2 decades, there have been tremendous breakthroughs in our understanding of how type II and type III cells detect molecules described by humans as sweet, bitter, umami, and sour, respectively. Type II and type III TBCs have been implicated in salt detection through amiloride-

insensitive mechanisms (Oka et al., 2013; Lewandowski et al., 2016; Roebber et al., 2019), but the identification of the TBC type (type I, II, or III) responsible for amiloride-sensitive salt detection remains elusive.

Studying the physiology of the taste system in isolation from other sensory systems present in the oral cavity is a challenging endeavor and has likely impeded our understanding of the cells involved in salt detection. Stimulating the oral cavity with concentrated solutions can produce unwanted confounds, such as increased osmotic pressure and activation of additional sensory systems (e.g., somatosensory and olfactory). Therefore, we took an optogenetic approach to investigate type I glial-like TBC taste physiology and role in behavior, as the light stimulus is devoid of the aforementioned confounds. GAD65 is selectively expressed in type I TBCs, so we took advantage of this by driving ChR2 and EYFP under the GAD65 promoter. Consistent with previous immunohistochemical reports, we found that GAD65-ChR2-EYFP was selectively expressed in NTPDase2 cells, which do not overlap with markers for type II and type III cells (Bartel et al., 2006; Dvoryanchikov et al., 2011).

In the taste system, epithelial sodium channels (ENaCs) have been regarded as the principal ion channels underlying amiloride-sensitive Na^+ transduction, but the expression of ENaC subunits in taste epithelium is widespread (Lin et al., 1999; Lossow et al., 2020b). The αENaC subunit is necessary for Na^+ transduction, but it is also expressed in type III cells, where it appears to be nonfunctional (Chandrashekar et al., 2010). Yoshida et al. (2009) showed that amiloride-sensitive TBCs coexpressed α, β, and γ subunits, whereas Lossow et al. (2020b) reported nonoverlapping expression patterns of ENaC subunits in TBCs and showed that type I cells express βENaC.

Dissociated fungiform cells expressing calcium homeostasis modulator 1 (CALHM-1) have amiloride-sensitive currents (Bigiani, 2017). Nomura et al. (2020) showed that CALHM-1 cells expressing αENaC were unresponsive to extracellular Na^+ when amiloride was present in the bath (Nomura et al., 2020). Interestingly, dissociated TBCs that were electrophysiologically identified as type I cells were also amiloride sensitive (Vandenbeuch et al., 2008)—yet, type I cells only express the βENaC subunit (Lossow et al., 2020b). By driving the expression of ChR2 into GAD65$^+$ cells, we were able to access their role in physiology and behavior directly, independent of whether they express α, β, and/or γ ENaC subunits.

We focused our attention on TBCs in fungiform papillae, located on the anterior tongue, as chorda tympani neurons innervating this region are critical for normal salt detection (Spector et al., 1990), salt discrimination, (Spector and Grill, 1992; Blonde et al., 2010), and Na^+ appetite (Breslin et al., 1993; O'Keefe et al., 1994; Markison et al., 1995; Roitman and Bernstein, 1999). We found that optogenetic stimulation of type I GAD65$^+$ TBCs in fungiform papillae increased the activity of peripheral and central gustatory neurons in a dose-dependent manner. Consistent with our hypothesis, N neurons, which responded best to NaCl through a benzamil-sensitive mechanism, were most sensitive to light across the intensity range. Furthermore, N neurons responded faithfully (90%) to a stimulation frequency (10 Hz) that was similar to the maximum lick rates (8–9 Hz) of C57BL/6J mice (Glatt et al., 2016; Raymond et al., 2018).

An interesting finding was that optogenetic stimulation of GAD65$^+$ TBCs also activated S and SQ neurons, which responded best to sucrose, as well as A neurons, which responded best to NH_4Cl. Compared with N neurons, however, S, SQ, and A neurons were less sensitive to light and responded less faithfully to light at 10 Hz, which may have important implications for neural coding during active licking. A number of taste-responsive neurons in the NTS are capable of following licks (Roussin et al., 2012), but it is often difficult to separate somatosensory (mechanosensory, proprioceptive, or thermal) from gustatory signals in awake-behaving animals. We found that optogenetic stimulation of GAD65$^+$ TBCs neither activated nor influenced mechanosensory neurons that innervated the anterior tongue. Thus, it appears that the ability of N neurons to follow light is most likely a gustatory signal.

For all neuron types, increasing the power of light resulted in increased spike activity and decreased response latency, which is consistent with how peripheral gustatory neurons respond to increasing stimulus concentration (Breza et al., 2010; Breza and Contreras, 2012a,b). Breadth of tuning in gustatory neurons also increases with stimulus concentration (Wu et al., 2015). The fact that S, SQ, and A neurons in the NTS responded to light at all, strongly suggests that some level of cross talk exists in the taste system, since ChR2 was not expressed in PLCβ2 or CA4 TBCs. It is possible that this occurs within the taste bud where GAD65$^+$ TBCs influence the activity of other TBCs in a paracrine-like fashion (Dando and Roper, 2009). This seems probable based on their glial-like morphology—essentially "hugging" other TBC types. It is also possible that this "cross talk" is the result of convergence of papillae onto peripheral nerve fibers (Miller, 1971) and/or central neurons in the NTS (Hill et al., 1983; Vogt and Mistretta, 1990).

We reasoned that if the pathway from GAD65$^+$ cells to N neurons was more direct (GAD65$^+$ TBCs → NaCl-best fibers → N neurons in NTS), then their latency to light would be short and faithful. If, however, the pathway from GAD65$^+$ TBCs to S, SQ, or A neurons was more indirect, such as the result of paracrine signaling (GAD65$^+$ TBCs → type II or type III cells → sucrose-best or NH_4Cl-best fibers → S, SQ, A neurons in NTS) or synaptic convergence, then response latencies to light would be longer and more variable. Contrary to our predictions, response latencies to light under our experimental conditions were not significantly different across neuron types. Although nonsignificant, N neurons had the shortest average response latency to light (see Results).

Gustatory neurons showed increased jitter in response to light stimulation at 10 Hz, which is in agreement with a complex polysynaptic system (Doyle and Andresen, 2001). The manner by which TBCs communicate with each other through paracrine signals (Dando and Roper, 2009) and with gustatory afferents via ATP (Finger et al., 2005) is complex, as there are traditional and nontraditional synapses (Taruno et al., 2013). It is possible that GAD65$^+$ TBCs communicate with an unidentified TBC type (possibly ENaCα CALHM1/3$^+$; Nomura et al., 2020) before communicating with NaCl-best afferents and then onto N neurons in the NTS. Certainly, the significant increase in jitter is evidence of complex signaling (Doyle and Andresen, 2001). Clearly there are many unanswered questions regarding the circuitry within the taste bud and how this impacts signals that are relayed to the gustatory NTS. Recordings from peripheral gustatory neurons simultaneous with optogenetic stimulation of TBC types will help our understanding of the nature and purpose of cell-to-cell communication.

Our behavioral findings validate our neurophysiological studies by demonstrating that the stimulation of GA65$^+$ TBCs has behavioral relevance. We quantified drinking behaviors that were driven by NaCl taste and "light taste." As expected from previous studies (Caloiero and Lundy, 2004; Raymond et al.,

2017; Lossow et al., 2020a), Na^+ depletion via amiloride self-administration resulted in a robust NaCl appetite. Na^+-depleted mice preferred to optogenetically stimulate GAD65$^+$ TBCs, which resulted in overconsumption of illuminated H_2O, despite exacerbating their Na^+ imbalance in the process. These same mice were indifferent to optogenetic stimulation when Na^+ replete. These behaviors largely recapitulate Na^+ appetite; Na^+ depletion drives a voracious appetite for NaCl, independent of thirst. When given the choice between NaCl and KCl, Na^+-depleted rats show a robust appetite for NaCl over KCl, and blockade of amiloride/benzamil-sensitive neurons, or transection of the chorda tympani nerve, disrupts this behavior (Roitman and Bernstein, 1999).

Optogenetic stimulation of GAD65$^+$ TBCs was sufficient to drive an appetite for light taste in a Na^+-depleted state, but that does not imply that GAD65$^+$ TBCs are necessary for Na^+ transduction. While optogenetic stimulation of GAD65$^+$ TBCs elicits consummatory behavior, consistent with Na^+ appetite, we cannot be certain of its perceived taste quality. It seems probable that optogenetic stimulation of GAD65$^+$ TBCs engaged a homeostatic reflex for Na^+ consumption, without bearing all the perceived qualities of a NaCl solution. Our behavioral assays were not designed to test whether optogenetic stimulation of GAD65$^+$ cells evokes a pure NaCl taste. More sophisticated psychophysical paradigms, such as those used to discriminate salts (St John et al., 1995; Spector et al., 1996), and basic taste qualities (Grobe and Spector, 2008) will be necessary to determine whether optogenetic stimulation of GAD65$^+$ TBCs leads to the perception of more than one taste quality. Optogenetic examination of other TBCs will be useful tools to understand the cross talk that seems to form the basis of side-band taste responses. Such experiments will shed light on our understanding of coding in the taste system.

References

Bartel DL, Sullivan SL, Lavoie EG, Sévigny J, Finger TE (2006) Nucleoside triphosphate diphosphohydrolase-2 is the ecto-ATPase of type I cells in taste buds. J Comp Neurol 497:1–12.

Benjamini Y, Hochberg Y (1995) Controlling the false discovery rate: a practical and powerful approach to multiple testing. J R Stat Soc Series B Stat Methodol 57:289–300.

Bigiani A (2017) Calcium homeostasis modulator 1-like currents in rat fungiform taste cells expressing amiloride-sensitive sodium currents. Chem Senses 42:343–359.

Blonde G, Jiang E, Garcea M, Spector AC (2010) Learning-based recovery from perceptual impairment in salt discrimination after permanently altered peripheral gustatory input. Am J Physiol Regul Integr Comp Physiol 299:R1027–R1036.

Boggs K, Venkatesan N, Mederacke I, Komatsu Y, Stice S, Schwabe RF, Mistretta CM, Mishina Y, Liu HX (2016) Contribution of underlying connective tissue cells to taste buds in mouse tongue and soft palate. PLoS One 11:e0146475.

Breslin PA, Spector AC, Grill HJ (1993) Chorda tympani section decreases the cation specificity of depletion- induced sodium appetite in rats. Am J Physiol 264:R319–R323.

Breza JM, Contreras RJ (2012a) Acetic acid modulates spike rate and spike latency to salt in peripheral gustatory neurons of rats. J Neurophysiol 108:2405–2418.

Breza JM, Contreras RJ (2012b) Anion size modulates salt taste in rats. J Neurophysiol 107:1632–1648.

Breza JM, Travers SP (2016) P2X2 receptor terminal field demarcates a "transition zone" for gustatory and mechanosensory processing in the mouse nucleus tractus solitarius. Chem Senses 41:515–524.

Breza JM, Curtis KS, Contreras RJ (2006) Temperature modulates taste responsiveness and stimulates gustatory neurons in the rat geniculate ganglion. J Neurophysiol 95:674–685.

Breza JM, Curtis KS, Contreras RJ (2007) Monosodium glutamate but not linoleic acid differentially activates gustatory neurons in the rat geniculate ganglion. Chem Senses 32:833–846.

Breza JM, Nikonov AA, Contreras RJ (2010) Response latency to lingual taste stimulation distinguishes neuron types within the geniculate ganglion. J Neurophysiol 103:1771–1784.

Caloiero VG, Lundy RF (2004) A novel method for induction of salt appetite in rats. Brain Res Bull 64:1–7.

Chandrashekar J, Kuhn C, Oka Y, Yarmolinsky DA, Hummler E, Ryba NJ, Zuker CS (2010) The cells and peripheral representation of sodium taste in mice. Nature 464:297–301.

Cohen J (1988) Statistical power analysis for the behavioral sciences, Ed 2. Mahwah, NJ: Erlbaum.

Cohen J (1992) A power primer. Psychol Bull 112:155–159.

Contreras RJ, Beckstead RM, Norgren R (1982) The central projections of the trigeminal, facial, glossopharyngeal and vagus nerves: an autoradiographic study in the rat. J Auton Nerv Syst 6:303–322.

Dando R, Roper SD (2009) Cell-to-cell communication in intact taste buds through ATP signalling from pannexin 1 gap junction hemichannels. J Physiol 587:5899–5906.

Doyle MW, Andresen MC (2001) Reliability of monosynaptic sensory transmission in brain stem neurons in vitro. J Neurophysiol 85:2213–2223.

Dvoryanchikov G, Huang YA, Barro-Soria R, Chaudhari N, Roper SD (2011) GABA, its receptors, and GABAergic inhibition in mouse taste buds. J Neurosci 31:5782–5791.

Finger TE, Danilova V, Barrows J, Bartel DL, Vigers AJ, Stone L, Hellekant G, Kinnamon SC (2005) ATP signaling is crucial for communication from taste buds to gustatory nerves. Science 310:1495–1499.

Geran LC, Spector AC (2000) Amiloride increases sodium chloride taste detection threshold in rats. Behav Neurosci 114:623–634.

Geran LC, Spector AC (2004) Anion size does not compromise sodium recognition by rats after acute sodium depletion. Behav Neurosci 118:178–183.

Geran LC, Spector AC (2007) Amiloride-insensitive units of the chorda tympani nerve are necessary for normal ammonium chloride detectability in the rat. Behav Neurosci 121:779–785.

Geran LC, Travers SP (2006) Single neurons in the nucleus of the solitary tract respond selectively to bitter taste stimuli. J Neurophysiol 96:2513–2527.

Glatt RA, St John SJ, Lu L, Boughter JD Jr (2016) Temporal and qualitative dynamics of conditioned taste aversions in C57BL/6J and DBA/2J mice self-administering LiCl. Physiol Behav 153:97–108.

Gleiberman L (1973) Blood pressure and dietary salt in human populations. Ecol Food Nutr 2:143–156.

Grobe CL, Spector AC (2008) Constructing quality profiles for taste compounds in rats: a novel paradigm. Physiol Behav 95:413–424.

Hill DL, Bradley RM, Mistretta CM (1983) Development of taste responses in rat nucleus of solitary tract. J Neurophysiol 50:879–895.

Hill DL, Formaker BK, White KS (1990) Perceptual characteristics of the amiloride-suppressed sodium chloride taste response in the rat. Behav Neurosci 104:734–741.

Huang AL, Chen X, Hoon MA, Chandrashekar J, Guo W, Tränkner D, Ryba NJ, Zuker CS (2006) The cells and logic for mammalian sour taste detection. Nature 442:934–938.

Kalyanasundar B, Blonde GD, Spector AC, Travers SP (2020) Electrophysiological responses to sugars and amino acids in the nucleus of the solitary tract of type 1 taste receptor double-knockout mice. J Neurophysiol 123:843–859.

Lemon CH, Margolskee RF (2009) Contribution of the T1r3 taste receptor to the response properties of central gustatory neurons. J Neurophysiol 101:2459–2471.

Lewandowski BC, Sukumaran SK, Margolskee RF, Bachmanov AA (2016) Amiloride-insensitive salt taste is mediated by two populations of type III taste cells with distinct transduction mechanisms. J Neurosci 36:1942–1953.

Lin W, Finger TE, Rossier BC, Kinnamon SC (1999) Epithelial Na+ channel subunits in rat taste cells: localization and regulation by aldosterone. J Comp Neurol 405:406–420.

Lossow K, Meyerhof W, Behrens M (2020a) Sodium imbalance in mice results primarily in compensatory gene regulatory responses in kidney and colon, but not in taste tissue. Nutrients 12:995.

Lossow K, Hermans-Borgmeyer I, Meyerhof W, Behrens M (2020b) Segregated expression of ENaC subunits in taste cells. Chem Senses 45:235–248.

Lu B, Breza JM, Nikonov AA, Paedae AB, Contreras RJ (2012) Leptin increases temperature-dependent chorda tympani nerve responses to sucrose in mice. Physiol Behav 107:533–539.

Lu B, Breza JM, Contreras RJ (2016) Temperature influences chorda tympani nerve responses to sweet, salty, sour, umami, and bitter stimuli in mice. Chem Senses 41:727–736.

Lundy RF Jr, Contreras RJ (1999) Gustatory neuron types in rat geniculate ganglion. J Neurophysiol 82:2970–2988.

Markison S, St John SJ, Spector AC (1995) Glossopharyngeal nerve transection does not compromise cation specificity of depletion-induced sodium appetite in rats. Am J Physiol 269:R215–R221.

Miller IJ Jr (1971) Peripheral interactions among single papilla inputs to gustatory nerve fibers. J Gen Physiol 57:1–25.

Ninomiya Y, Tonosaki K, Funakoshi M (1982) Gustatory neural response in the mouse. Brain Res 244:370–373.

Nomura K, Nakanishi M, Ishidate F, Iwata K, Taruno A (2020) All-electrical Ca(2+)-independent signal transduction mediates attractive sodium taste in taste buds. Neuron 106:816–829.e6.

Oka Y, Butnaru M, von Buchholtz L, Ryba NJ, Zuker CS (2013) High salt recruits aversive taste pathways. Nature 494:472–475.

O'Keefe GB, Schumm J, Smith JC (1994) Loss of sensitivity to low concentrations of NaCl following bilateral chorda tympani nerve sections in rats. Chem Senses 19:169–184.

Raymond MA, Chowdhury T, Mast TG, Breza JM (2017) A simple method for a rapid induction of salt appetite in mice. Paper presented at AChemS XXXIX, 39 Annual Meeting of the Association for Chemoreception Sciences, Bonita Springs, FL, April.

Raymond MA, Mast TG, Breza JM (2018) An open-source lickometer and microstructure analysis program. HardwareX 4:e00035.

Roebber JK, Roper SD, Chaudhari N (2019) The role of the anion in salt (NaCl) detection by mouse taste buds. J Neurosci 39:6224–6232.

Roitman MF, Bernstein IL (1999) Amiloride-sensitive sodium signals and salt appetite: multiple gustatory pathways. Am J Physiol 276:R1732–R1738.

Roussin AT, D'Agostino AE, Fooden AM, Victor JD, Di Lorenzo PM (2012) Taste coding in the nucleus of the solitary tract of the awake, freely licking rat. J Neurosci 32:10494–10506.

Schnorr JA, Brookshire KH (1965) Distilled water and tap water as factors in taste preference experimentation. Psychol Rep 17:191–194.

Smith DV, Travers JB (1979) A metric for the breadth of tuning of gustatory neurons. Chem Senses 4:215–229.

Spector AC, Grill HJ (1992) Salt taste discrimination after bilateral section of the chorda tympani or glossopharyngeal nerves. Am J Physiol 263:R169–R176.

Spector AC, Travers SP (2005) The representation of taste quality in the mammalian nervous system. Behav Cogn Neurosci Rev 4:143–191.

Spector AC, Schwartz GJ, Grill HJ (1990) Chemospecific deficits in taste detection after selective gustatory deafferentation in rats. Am J Physiol 258:R820–R826.

Spector AC, Guagliardo NA, St John SJ (1996) Amiloride disrupts NaCl versus KCl discrimination performance: implications for salt taste coding in rats. J Neurosci 16:8115–8122.

St John SJ, Markison S, Spector AC (1995) Salt discriminability is related to number of regenerated taste buds after chorda tympani nerve section in rats. Am J Physiol 269:R141–R153.

Taruno A, Vingtdeux V, Ohmoto M, Ma Z, Dvoryanchikov G, Li A, Adrien L, Zhao H, Leung S, Abernethy M, Koppel J, Davies P, Civan MM, Chaudhari N, Matsumoto I, Hellekant G, Tordoff MG, Marambaud P, Foskett JK (2013) CALHM1 ion channel mediates purinergic neurotransmission of sweet, bitter and umami tastes. Nature 495:223–226.

Teng B, Wilson CE, Tu YH, Joshi NR, Kinnamon SC, Liman ER (2019) Cellular and neural responses to sour stimuli require the proton channel Otop1. Curr Biol 29:3647–3656.e5.

Vandenbeuch A, Clapp TR, Kinnamon SC (2008) Amiloride-sensitive channels in type I fungiform taste cells in mouse. BMC Neurosci 9:1.

Vogt MB, Mistretta CM (1990) Convergence in mammalian nucleus of solitary tract during development and functional differentiation of salt taste circuits. J Neurosci 10:3148–3157.

Whiddon ZD, Rynberg ST, Mast TG, Breza JM (2018) Aging decreases chorda-tympani nerve responses to NaCl and alters morphology of fungiform taste pores in rats. Chem Senses 43:117–128.

Wilson DM, Boughter JD Jr, Lemon CH (2012) Bitter taste stimuli induce differential neural codes in mouse brain. PLoS One 7:e41597.

Wu A, Dvoryanchikov G, Pereira E, Chaudhari N, Roper SD (2015) Breadth of tuning in taste afferent neurons varies with stimulus strength. Nat Commun 6:8171.

Yoshida R, Horio N, Murata Y, Yasumatsu K, Shigemura N, Ninomiya Y (2009) NaCl responsive taste cells in the mouse fungiform taste buds. Neuroscience 159:795–803.